PRODUCTION AND CHARACTERIZATION OF POLYLACTIDE/SILVER NANOWIRE NANOCOMPOSITE FILMS

A THESIS SUBMITTED TO
THE GRADUATE SCHOOL OF NATURAL AND APPLIED SCIENCES
OF
MIDDLE EAST TECHNICAL UNIVERSITY

BY

DOĞA DOĞANAY

IN PARTIAL FULFILLMENT OF THE REQUIREMENTS
FOR
THE DEGREE OF MASTER OF SCIENCE
IN
METALLURGICAL AND MATERIALS ENGINEERING

SEPTEMBER 2016

Approval of the thesis:

PRODUCTION AND CHARACTERIZATION OF POLYLACTIDE/SILVER NANOWIRE NANOCOPOSITE FILMS

submitted by **DOĞA DOĞANAY** in partial fulfillment of the requirements for the degree of **Master of Science in Metallurgical and Materials Engineering Department, Middle East Technical University** by,

Prof. Dr. Gülbin Dural Ünver _____
Dean, Graduate School of **Natural and Applied Sciences**

Prof. Dr. C. Hakan Gür _____
Head of Department, **Metallurgical and Materials Engineering**

Assoc. Prof. Dr. H. Emrah Ünalan _____
Advisor, **Metallurgical and Materials Eng. Dept., METU**

Prof. Dr. Cevdet Kayak _____
Co-advisor, **Metallurgical and Materials Eng. Dept., METU**

Examining Committee Members:

Prof. Dr. Cevdet Kaynak _____
Metallurgical and Materials Engineering Dept., METU

Assoc. Prof. Dr. Hüsnü Emrah Ünalan _____
Metallurgical and Materials Engineering Dept., METU

Assoc. Prof. Dr. Emren Nalbant Esentürk _____
Dept. Chemistry., METU

Assist. Prof. Dr. Mert Efe _____
Metallurgical and Materials Engineering Dept., METU

Prof. Dr. Atilla Cihaner _____
Chemical Engineering and Applied Chemistry Dept., Atılım Uni.

Date: 01.09.2016

I hereby declare that all information in this document has been obtained and presented in accordance with academic rules and ethical conduct. I also declare that, as required by these rules and conduct, I have fully cited and referenced all material and results that are not original to this work.

Name, Last name: Doğa Doğanay

Signature :

ABSTRACT

PRODUCTION AND CHARACTERIZATION OF POLYLACTIDE/SILVER NANOWIRE NANOCOMPOSITE FILMS

Doğanay, Doğa

M.S., Department of Metallurgical and Materials Engineering

Advisor: Assoc. Prof. Dr. H. Emrah Ünalan

Co-advisor: Prof. Dr. Cevdet Kaynak

September 2016, 59 pages

In this theses, electrically conductive silver nanowire (Ag NW) filled polylactide (PLA) nanocomposites were fabricated and characterized. Ag NWs/PLA nanocomposite films were fabricated using simple solution mixing method and casted onto glass substrates via doctor blading. Following the obtainment of free standing nanocomposites through peeling off, electrical conductivity of the fabricated nanocomposites, interfacial interactions between Ag NWs and PLA as well as nanocomposite morphology, degree of alignment of Ag NWs, transition temperature and crystallinity among with mechanical performance were investigated. Nanowires showed good dispersion within the PLA matrix. Due to their high aspect ratio (≈150), a percolation threshold of 0.13 vol.% was measured for the nanocomposites. Conductivity of the nanocomposites at the maximum loading (1.74 vol.%) was measured as 27 S/m. It was also found that the transition temperatures of PLA matrix remain the same following the formation of nanocomposites.

Keywords: Polymer-matrix composites (PMCs), Nano-structures, Electrical properties, Mechanical properties.

,

ÖZ

POLİLAKTİT/GÜMÜŞ NANOTEL NANOKOMPOZİT FİLMLERİN ÜRETİMİ VE KARAKTERİZASYONU

Doğanay, Doğa

Yüksel Lisans, Metalurji ve Malzeme Mühendisliği Bölümü

Tez Danışmanı: Doç. Dr. H. Emrah Ünalan

Ortak Tez Danışmanı: Prof. Dr. Cevdet Kaynak

Eylül 2016, 59 sayfa

Bu tezde gümüş nanotel (Ag NW) katkılı polylaktik asit (PLA) matrisli iletken nanokompoziter üretilmiş ve karaterize edilmiştir. Ag NW/PLA nanokompozit filmler çözelti karıştırma yöntemi ile üretilmiş ve doktor blade yöntemiyle cam altlıkların üzerine dökülmüştür. Nanokompozit filmler cam yüzeylerinden kaldırıldıktan sonra elektriksel ilketkenlikleri, iç yapıları, nanotellerin iç yapı içerisindeki yönelimleri, mekanik özellikleri, kristallenme davranışları ve nanotellerle polimer matrisin arayüzey etkileşimleri incelenmiştir. Nanotellerin matris içerisinde iyi bir dağılım gösterdiği gözlenmiştir. Nanoteller yüksek boy çap orarına (≈150) sahip oldukları için, elektrik iletkenliği için perkolasyon eşik değeri, hacimce 0.13% olarak ölçülmüştür. Bu nanokompozit filmlerin elektriksel iletkenliği, maksimum nanotel katkısında (hacimce 1.74 %) 27 S/m olarak ölçülmüştür. Nanokompozitlerin kritik geçiş sıcaklıkları ise herhangi bir değişim göstermemiştir.

Anahtar Kelimeler: Polilaktik asit (PLA), gümüş nanotel (Ag NW), nanokompozit.

To My Family

ACKNOWLEDGEMENTS

Firstly, I would like to express my deepest gratitude to my advisor Assoc. Prof. Dr. H. Emrah Ünalan for his support, guidance and patience throughout the study. It is a great honor to work under his supervision. I also would like to thank my co-advisor Prof. Dr. Cevdet Kaynak for his supports and guidance.

Secondly, I would like to thank my friend and mentor Şahin Coşkun. This thesis would have never been completed without his guidance and support. I also would like to thank my lab mates Mete Batuhan Durukan, Sevim Polat, Ece Alpugan, Ayşegül Afal, Onur Türel, Alptekin Aydınlı, İpek Bayraktar, Itır Bakış Doğru, Doğancan Tigan, Pantea Aurang, Ekim Saraç, Can Çuhadar and Recep Yüksel. They all will be remembered for their intimate friendship. Also, special thanks to Dr. Mehmet Yıldırım and Serkan Yılmaz for their support to my studies.

I want to thank my friend Eyüp Can Demir, especially for his supports which encouraged me to start my graduate studies. He will also be in my memory with joyful moments that we were together in our undergraduate years.

Most importantly, I want to thank my lovely girlfriend Tuba Yakar. She always shows unconditional support, patience and most importantly her love.

At last, I would like to thank my mother, my father, and my sister. As a scientist and human being, every achievement I made is a result of their effort. I love you.

TABLE OF CONTENTS

ABSTRACT ……..V

ÖZ……VII

ACKNOWLEDGEMENTS…….....IX

TABLE OF CONTENTS……XI

LIST OF TABLES……..XV

LIST OF FIGURES…….....XVII

CHAPTERS

1. INTRODUCTION……..1

2. LITERATURE REVIEW……..5

2.1.Polylactide……..……5

2.1.1.Production of Polylactide……5

2.1.2. Properties of Polylactide……..7

2.1.2.1. Physical and Thermal Properties…….8

2.1.2.2. Mechanical Properties…….9

2.1.3. Electrically Conductive PLA Matrix Nanocomposites…….10

2.1.3.1. Nanofillers……10

2.1.3.2. Carbon Based Nanofillers……11

2.1.3.2.1. Carbon Nanotubes/PLA Nanocomposites…..12

2.1.3.2.2. Graphene/PLA Nanocomposites……....12

2.1.3.2.3. Silver Nanoparticle/PLA Nanocomposites…14

2.2. Silver Nanowire……...14

2.2.1 Polyol Sythesis of Silver Nanowires……14

2.2.2. Silver Nanowire Reinforced Polymer Matrix Nanocomposites……16

3. EXPERIMENTAL DETAILS…….27

3.1. Materials Used…….27

3.1.1. Matrix Polymer (PLA)……..27

3.2. Ag NW Synthesis and Nanocomposite Production……..……...27

3.2.1. Ag NW Synthesis……..……...27

3.2.2. Preperation of Nanocomposite Films……....……..28

3.3. Characterizaion of Ag NWs and Nanocomposite Films…….…...…..29

3.3.1. Transmittance Measurements……...29

3.3.2. Scanning Electron Microscopy (SEM) Analysis……..29

3.3.3. Thermogravimetric Analysis (TGA)…….....29

3.3.4. Differantial Scanning Calorimeter (DSC)…….29

3.3.5. Fourier Transformed Infrared (FTIR) Spectroscopy…….30

3.3.6. Electrical Conductivity Measurements.…….……...30

3.3.7. Tensile Tests.…….……...30

4. RESULTS AND DISCUSSIONS..……...33

4.1.SEM Analysis……...33

4.1.1. Determination of Ag NW Morphology…….33

4.1.2. Distribution of Ag NWs within the Matrix……...34

4.1.1. Alignment of Ag NWs within the Matrix…….....35

4.2.Thermal Properties……...36

4.2.1. Thermogravimetric Analysis (TGA)…….36

4.2.2. Differantial Scanning Calorimeter (DSC)…….....38

4.3.Interfacial Interaction Between Ag NWs and PLA……..40

4.4.Electrical Conductivity…….....41

4.3.Mechanical Properties……...45

5. CONCLUSIONS AND FUTURE RECOMMEDATIONS……...49

5.1.Conclusions ……..49

5.2.Future Recommendations……..……..50

REFERENCES…….51

LIST OF TABLES

TABLES

Table 4.1. Parameters determined from TGA and DSC analysis……...38

Table 4.2. Positions and assignments of distinctive IR bands of PLA, Ag NW and fabricated nanocomposites……..42

Table 4.3. Mechanical performance comparisons of PLA matrix nanocomposites...48

LIST OF FIGURES

FIGURES

Figure 2.1. Chemical structures of L-Lactic acid and D-Lactid acid..……..5

Figure 2.2. Synthesis methods of PLA……..6

Figure 2.3. Polymerization of PLA via lactide formation and ring opening polymerization method…….7

Figure 2.4. Physical states of amorphous PLA at different temperaures……..8

Figure 2.5. Physical states of semicrystalline PLA at different temperaures……9

Figure 2.6. Comparison of mechanical properties of conventional plastics in comparison to PLA……..10

Figure 2.7. Schematic representations of 0D, 1D, and 2D nanostructures…….11

Figure 2.8. (a) Low magnifications and, (b) High magnification TEM images of graphene……..13

Figure 2.9. Schematic representation of (a) an individual NW growth from the penta twin particle. The tips of the nanowire are {111}, the side surfaces of the NW are {100} planes of FCC structure. The strong PVP interaction with {111} planes are represented with dark-gray whereas the weak interaction with {100} planes are in blue color. The red lines indicate the twin boundaries, which can act as active sides for newly reduced Ag^{+} ions and (b) the diffusion of atoms to the active tips……...……15

Figure 2.10. (a-b) SEM images, (c) TEM image of electrodeposited Ag NWs……...16

Figure 2.11. Change in volume resistivity of the nanocomposites with respect to vol. % of (a) Ag NWs and (b) Cu NWs……...17

Figure 2.12. Change in resistance of Ag NW/PS nanocomposites with respect to temperature…….18

Figure 2.13. SEM images of the fractured surfaces of 3 vol. % (a) electrodeposited, (b) polyol synthesized Ag NW/P(VDF-TrFE) nanocomposites……..19

Figure 2.14. Volume electrical conductivity of both Ag NP and Ag NW filled P(VDF-TrFE) nanocomposites……20

Figure 2.15. Volume electrical conductivity of Ag NW/polyamide 11 nanocomposites. Inset is the conductivity versus Ag NW volume difference between an arbitrary and at the percolation content……...21

Figure 2.16. Change in (a) glass transition temperature and (b) % crystallinity with respect to Ag NW volume fraction……..22

Figure 2.17. Optical microscope images of (a) 0.04 (b) 0.16 and (c) 0.64 wt. % Ag NW included nanocomposite films. (d) SEM image of 1.73 wt% Ag NW/PC nanocomposite film…….23

Figure 2.18. Schematic representation of the latex blending method used to produce Ag NW/PS nanocomposites……24

Figure 2.19. Schematic representation of Ag NWs and SiO_2 NPs interface interactions……..25

Figure 3.1. (a) Schematic presentation of the doctor blading method investigated herein this work. (b) Photograph of Ag NWs suspended in PLA/chloroform solution……28

Figure 4.1. SEM images of (a) Ag NWs and (b) an individual Ag NW. Arrows point residual polymer layer on the lateral surface of the NWs…….33

Figure 4.2. Top-view SEM images of nanocomposites with Ag NW contents of (a) 0.13, (b) 0.66, (c) 1.74 vol. %. (d) Crosssectional SEM image of 0.66 vol.% Ag NW/PLA nanocomposite……34

Figure 4.3. (a) SEM image of 0.66 vol.% Ag NW/PLA nanocomposite film showing the angle between NWs and the blading direction. (b) <Cos2(θ)> values of nanocomposites with different Ag NW loading. Lines are for visual aid…….35

Figure 4.4. (a) Thermalgravimetric analysis of neat PLA and fabricated Ag NW/PLA nanocomposites and (b) SEM image of the TGA residue……37

Figure 4.5. (a) Second heating DSC thermograms of bare PLA and fabricated nanocomposites, (b) percent crystallinity of PLA and fabricated nanocomposites. Lines are for visual aid…….39

Figure 4.6. FTIR spectrum of the bare PLA, Ag NWs and 1.75 vol.% Ag NW/PLA nanocomposites……...41

Figure 4.7. Conductivity of the fabricated Ag NW/PLA nanocomposites with respect to Ag NW content……45

Figure 4.8. (a) Representative stress-strain curves of bare PLA and Ag NW/PLA nanocomposites. (b) Effects of Ag NW content on elastic modulus and tensile strength of the nanocomposites. (c) Cross-sectional SEM fractograph of 0.24 vol.% Ag NW/PLA nanocomposite……47

CHAPTER 1

INTRODUCTION

Electrically conductive polymer composites stand out with their application areas like antistatic packaging, transistors and heaters [1-3]. Besides these wide range of applications, easy processability is another advantage of the conducting polymer composites. There is a critical filler content where a three dimensional (3D) network starts to form in a polymer matrix creating a conductive path for electrical conduction, known as the percolation threshold [4]. In literature, several additives such as carbon black, metallic nanoparticles, carbon nanotubes (CNTs), metallic nanowires and graphene were investigated for the production of conductive polymer composites [5-13]. A minimum filler content of 5 and 14 vol. % for silver (Ag) nanoparticles and carbon black particles were reported, respectively, for percolation [5,6]. 3D networks require a higher filler content for additives like nanoparticles. However, high filler content deteriorates the mechanical properties of the matrix materials, in addition to increasing the viscosity of the mixture, which would in turn reduce the processability. One dimensional (1D) nanostructures, on the other hand, were reported to provide higher conductivity at lower filler fractions as opposed to nanoparticles [7]. For instance, CNT reinforced polymer matrix composites have been extensively studied with different matrix materials. The lowest percolation threshold was reported as 0.0025 wt. % for CNT/epoxy composites; however, the maximum obtained conductivity was 10^{-1} S/m, which is not enough for many electronic applications [8]. Therefore, fillers with higher intrinsic conductivity compared to CNTs are required to increase the obtained maximum conductivity from the nanocomposites. At this point, metallic nanowires (NW) appear as promising candidates. In fact, copper (Cu), nickel

(Ni) and Ag NWs have already been used as additives for different polymer matrices [9-11]. However, due to oxide layer formation on Cu and Ni NWs, maximum conductivity of the nanocomposites could not exceed 10^{-1} S/m [9,10]. In contrast, higher conductivity values were reported from the nanocomposites fabricated with Ag NWs [12,13].

Polymers synthesized from renewable sources received considerable attention due to their environmentally friendly characters [14]. In addition, scarcity of petroleum resources increased demands for alternative renewable raw materials [15]. In this context, biodegradable poly (lactic acid) (PLA) seems to be one of the best candidates among all biopolymers with its promising thermal and mechanical properties as well as low cost [16]. Due to these advantages, PLA has been used in a wide range of applications from food packaging to tissue engineering [16,17]. However, these properties still need to be improved for various other applications. For this purpose, different types of additives have been extensively studied. For instance, water vapor permeation and tensile properties of the PLA matrix nanocomposites have been improved through nanoclay addition [18]. In another case, metal nanoparticle/PLA composites were fabricated and their optical, antibacterial and catalytic properties were investigated [19]. Electrically conductive fillers like CNTs and graphene oxide have been also studied within the PLA matrix [20,21]. Moreover, PLA is the most widely used polymeric ink for 3D printers [22]. With that respect, 3D printed PLA scaffolds were produced and used for tissue regeneration [23]. In terms of the 3D printing of PLA nanocomposites, carbon black was used as a conductive filler for the fabrication of electronic sensors [24]. Graphene was also used as a conductive additive for the fabrication of 3D printed graphene/PLA nanocomposites and turned into a commercial product [25,26].

In this thesis, Ag NWs are used for the first time as conductive fillers within the PLA matrix. Ag NW/PLA nanocomposites were produced through simple doctor blading technique. Effects of Ag NW content on the percolation threshold, electrical conductivity and mechanical properties of the nanocomposites were investigated.

Important transition temperatures of the PLA matrix such as glass transition, degradation and crystallization temperatures, interfacial interactions between the PLA and Ag NWs, and degree of alignment of Ag NWs within the matrix were also examined.

CHAPTER 2

LITERATURE REVIEW

2.1. Polylactide

2.1.2. Production of Polylactide

Swedish chemist Scheele firstly isolated lactic acid form milk in 1780 and it was commercially produced in 1881 [27]. Chemical synthesis and fermentation are the two types of lactic acid production methods. Fermentation type of synthesis took considerable attention due to its low cost, environmentally friendly character and high purity of the products [28]. There are two isomers of lactic acid, which are D-lactic acid and L-lactic acid. The structure of these isomers are provided in Figure 2.1.

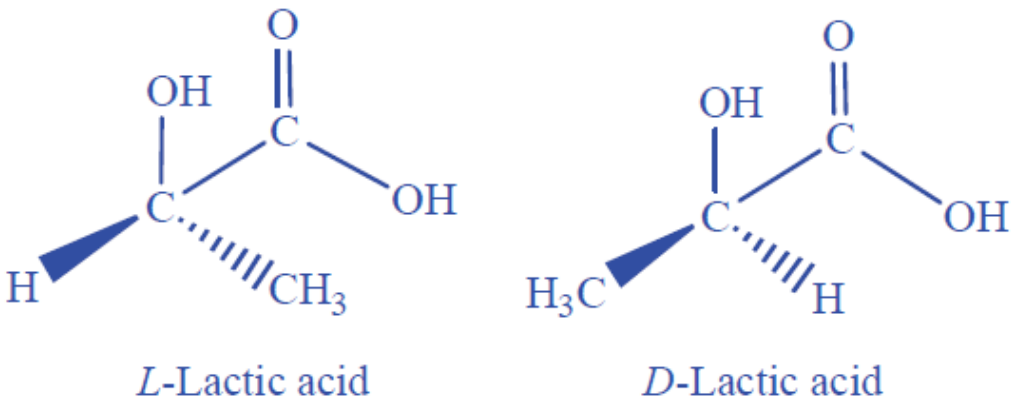

Figure 2.1. Chemical structures of L-Lactic acid (left) and D-Lactic acid (right) [29].

High molecular weight PLA can be synthesized via two different polymerization methods as shown in Figure 2.2. The first method is condensation polymerization of lactic acid. In this method, at first lactic acid is polymerized to a low molecular weight polymer. This low molecular weight polymer is useless due its brittle nature. Therefore, different coupling agents are used to increase the molecular weight. However, producing high molecular weight PLA with the condensation method is challenging because of high viscosity, existence of impurities within the product, difficulties in removal of water and low concentration of reactive end groups [30].

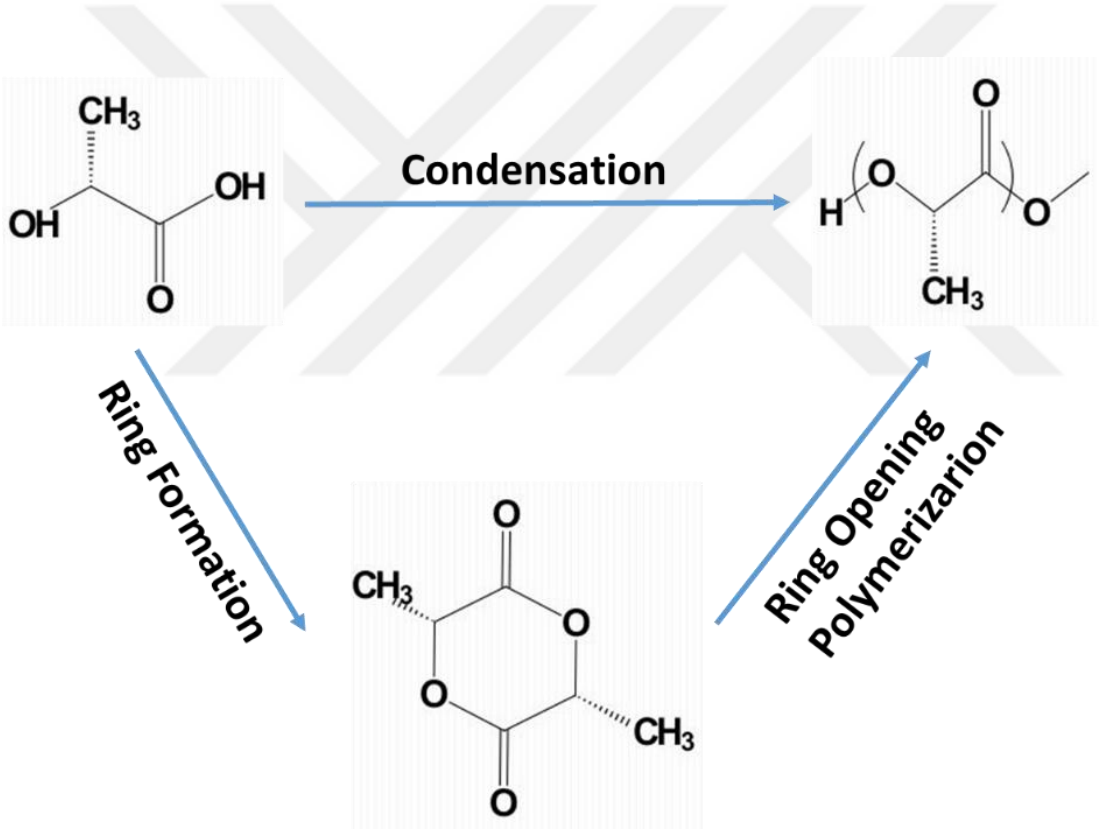

Figure 2.2. Synthesis methods of PLA. Adapted from [31].

The second and more frequently preferred method is polymerization through lactide ring formation followed by ring opening polymerization, which is schematically

summarized in Figure 2.3. At the first step of this method, D-lactic acid and/or L-lactic acid are polymerized to low molecular weight pre-polymer. Then, the pre-polymer is converted to lactide ring under low vacuum using a catalyst. Finally, the lactide rings are polymerized to the high molecular weight PLA via ring opening polymerization.

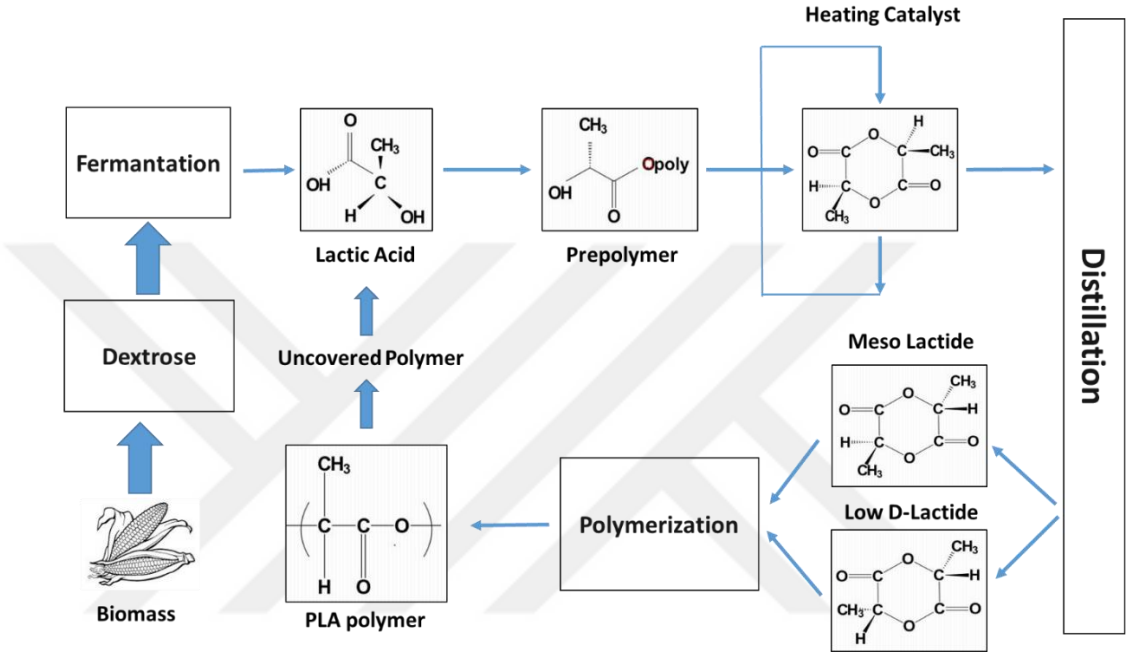

Figure 2.3. Polymerization of lactic acid via lactide formation and ring opening polymerization method. Adapted from [32].

2.1.2. Properties of PLA

The properties of PLA as well as any other polymers are directly related with the polymer architecture and its molecular mass. The architecture and molecular mass can be controlled via different methods during polymerization as briefly discussed in the previous section. Crystallinity percent, which is directly related with the processing parameters also effects these properties. Properties of PLA are described in this part of the thesis.

2.1.2.1. Physical and Thermal Properties

High molecular weight PLA can be either totally amorphous or partially crystalline at room temperature. These amorphous and partially crystalline structures depend on the monomer amounts in the structure. If there are more than 93 wt. % of L-lactic acid in the structure, PLA will be semicrystalline (percent crystallinity can be up to 40 %) [33,34]. On the other hand, if L-lactic acid content is less than 93 %, PLA will be totally amorphous.

Physical states and transition temperatures of amorphous PLA are shown in the Figure 2.4. β-relaxation temperature (T_β) is -45 ^{o}C. Below this temperature PLA is strictly brittle. Above the T_β side groups of the chains becomes mobile. Above the glass transition temperature (T_g), PLA becomes rubbery. T_g can be describe as the transition temperature at which polymer chains starts to slide each other. Between this transition temperatures, PLA can show both brittle and ductile character. Amorphous PLA becomes a viscous liquid between 110 and 150 ^{o}C. Decomposition temperature of the amorphous PLA is in the range of 215 ^{o}C and 285 ^{o}C.

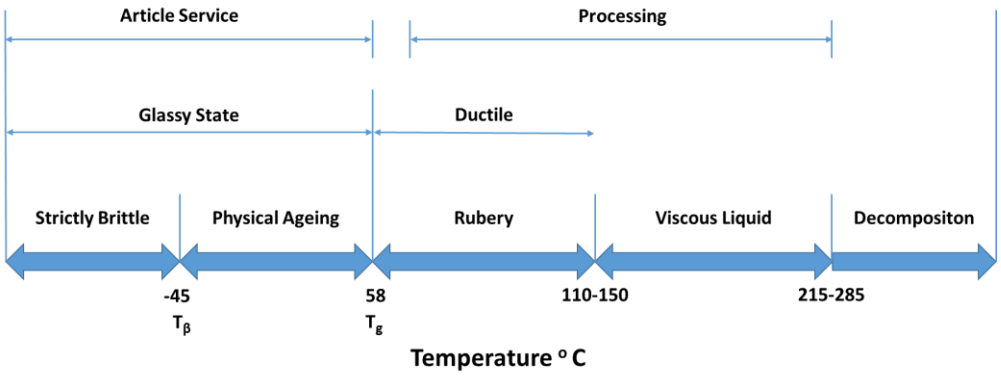

Figure 2.4: Physical states of amorphous PLA at different temperatures. Adapted from [34].

Transition temperatures and physical states of semicrystalline PLA are provided in Figure 2.5. Tg of semicrystalline PLA depends on its molecular weight and percent crystallinity and ranges from 58 to 70 ^{o}C. Below this transition temperature, PLA is brittle while it shows ductile character above this temperature. Melting temperature of semicrystalline PLA, which is between 130 and 207 ^{o}C, is slightly higher than the amorphous counterpart, as expected.

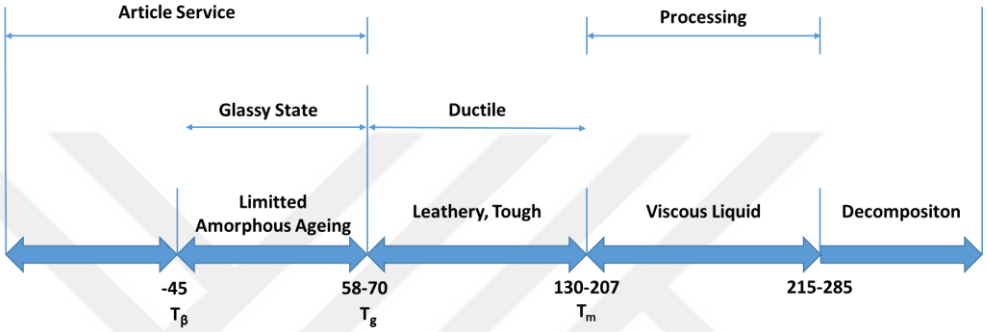

Figure 2.5: Physical states of semicrystalline PLA at different temperaures. Adapted from [34].

2.1.2.2. Mechanical Properties

Although PLA is a kind of biopolymer, it has high stiffness and strength. Therefore, it can compete with conventional petrochemical based polymers. Jacobsen and coworkers showed the potential of PLA to be an alternative for the conventional products [35]**.** Mechanical properties of PLA and other conventional plastics such as polypropylene (PP), high density polyethylene (HDPE) are compared in Figure 2.6. Young's modulus of PLA is 3.8 GPa, which is two times higher than that of HDPE. Tensile modulus of PLA is around 60 MPa and it is higher than many conventional plastics. However, percent elongation at fracture should be increased to utilize PLA for engineering applications. Therefore, many studies in literature aimed at increasing percent elongation of PLA.

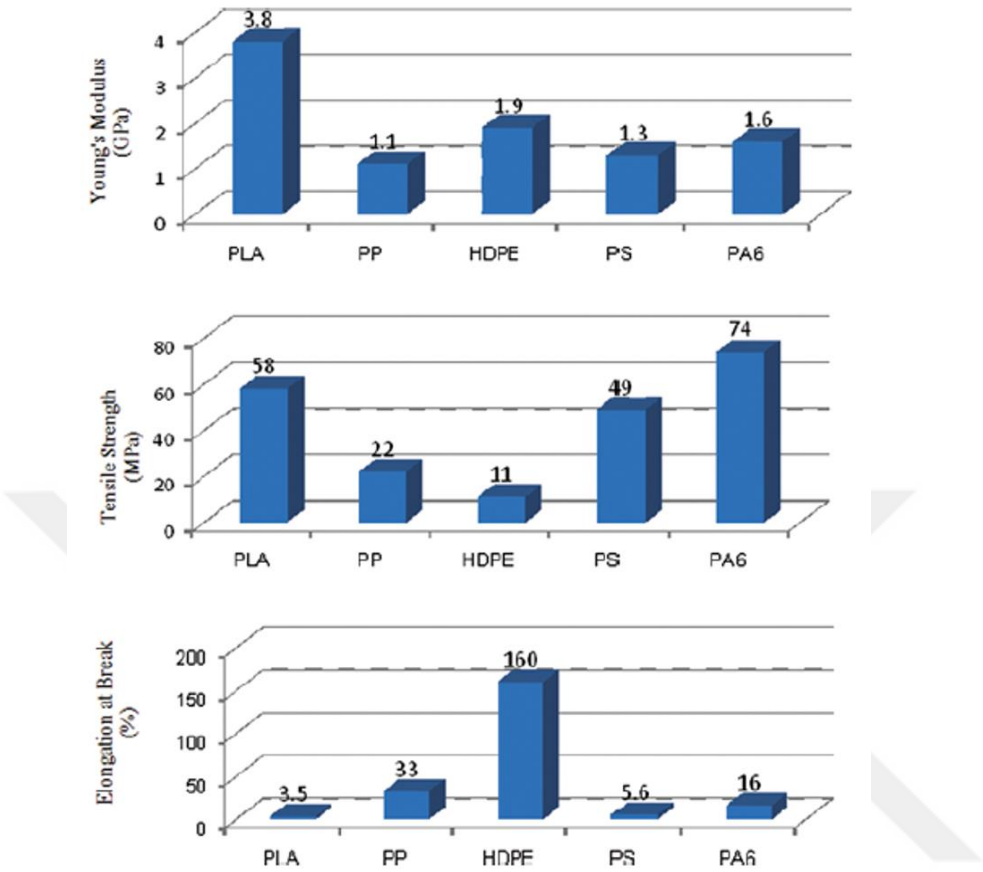

Figure 2.6. Comparison of mechanical properties of conventional plastics in comparison to PLA [36].

2.1.3. Electrically Conductive PLA Matrix Nanocomposites

2.1.3.1. Nanofillers

In Latin, nano means “dwarf” and one nanometer is one-billionth of a meter. In order to describe a material as nano, at least one dimension of it is needed to be smaller than 100 nm. In the last two decades, nanomaterials received considerable attention both in literature and industry. Because, at the nanoscale, materials start to show different properties than their bulk counterparts. There are basically two different approaches to fabricate nanomaterials, namely “top-down” and “bottom-up”. In the top down

approach, the dimensions of a bulk material are reduced down to the nanoscale with different techniques like chemical and mechanical etching. On the other hand, in the "bottom-up approach, atoms are assembled one-by-one to obtain nanomaterials. These two different approaches have many different advantages and disadvantages over each other. Apart from the fabrication approach, nanomaterials can also be specified with their geometry as zero, one and two dimensional (0D, 1D, 2D), which are schematically shown in Figure 2.7. All the three dimensions of 0D nanomaterials named as nanoparticles are the less than 100 nm. Two dimensions of 1D nanomaterials such as nanowires and nanotubes are less than 100 nm; whereas, only one dimension is less than 100 nm for 2D nanomaterials like graphene and nanosheets.

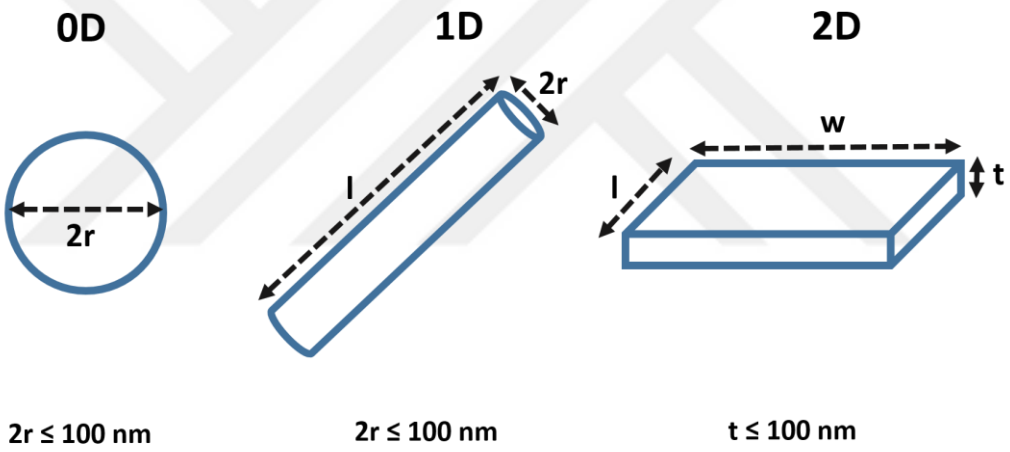

Figure 2.7. Schematic presentations of 0D, 1D and 2D nanostructures.

2.1.3.2. Carbon-Based Nanofillers

Carbon based nanostructures are widely used in literature within different matrices due to their high mechanical performance, electrical and thermal conductivity. Although there are several carbonaceous nanostructures, CNT and graphene are the two most frequently used fillers.

2.1.3.2.1. Carbon Nanotube/PLA Nanocomposites

Up to now, several conductive additives were used for the fabrication of electrically conductive PLA matrix nanocomposites. CNTs as 1D nanostructures are the most widely used nano additive for this purpose. In 2002, Bizios and coworkers used CNTs to produce PLA matrix nanocomposites for the first time and utilized this conductive composites to expose cells to electrical stimulation [37]. In another study, Kuan et al. investigated the amount of CNTs on the electrical conductivity of PLA. They showed that only 0.5 wt % CNT addition decrease surface resistivity for eight orders or magnitude [38]. Uniform dispersion of additives is one of the most important issues for nanocomposites. Villmow and coworkers investigated the influence of twin screw extrusion conditions on the dispersion of CNTs in the PLA matrix. They found that the percolation threshold for these nanocomposites is 0.5 wt.% CNTs in case of perfect dispersion [39]. Shape memory nanocomposites were produced using CNT/PLA nanocomposites by Raja and coworkers. These nanocomposites had a relatively high recovery ratio even after 50 bending cycles [40]. More recently, Wei et al. used CNT/PLA nanocomposites for chemical sensing. The effect of the CNT content on the response of the nanocomposites under different chemical vapors were investigated [41].

2.1.3.2.2. Graphene/PLA Nanocomposites

Graphene is a two dimensional nanostructure of carbon. It is an atomically thick material with sp^2 hybridized carbon atoms. Low and high magnification transmission electron microscope (TEM) images of graphene are provided in Figure 2.8 (a) and (b), respectively.

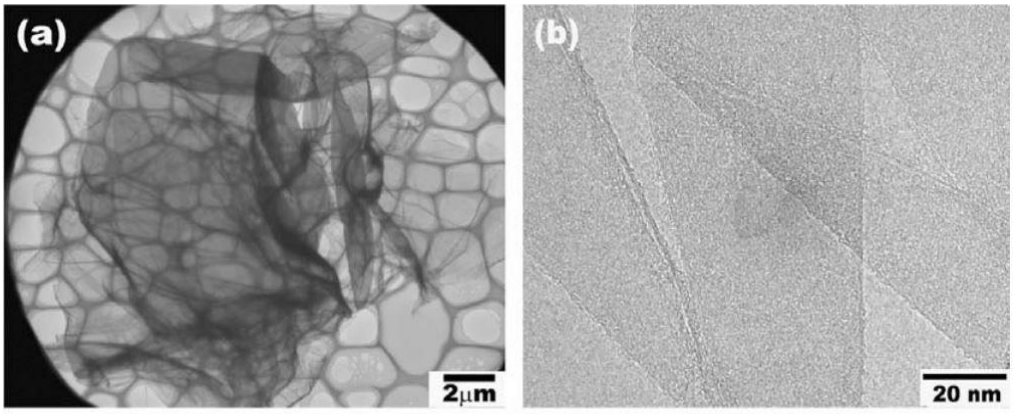

Figure 2.8. (a) Low magnification and (b) high magnification TEM images of graphene [43].

Since the discovery of graphene in 2004, it is widely used for different applications [42]. One of these applications is the fabrication of electrically conductive nanocomposites with graphene fillers for high mechanical and thermal performance. One of the most important issues for graphene reinforced nanocomposites is the dispersion control within the matrix. Instead of bundling as in the case of CNTs, limited exfoliation is the main problem for graphene. In order to solve this problem, different stabilization agents are used [44, 45]. Production of graphene reinforced PLA matrix nanocomposites were started in 2010. Kim and Jeong investigated the effect of graphene amount on the morphology, thermal stability, electrical conductivity and mechanical performance of PLA/graphene composites. They used melt compounding method for the production of nanocomposites. Percolation threshold was found to be 3 wt.%, which was lower than the other graphene/polymer matrix composites. The reason for this low percolation threshold was the acid treatment of graphene, which improve exfoliation and thus dispersion [46]. In the same year, another research group investigated the flame retardancy effect of graphene/PLA nanocomposites. Although some aggregations were present in the structure, flame retardancy effect of the nanocomposites were found to be quite promising [47].

2.1.3.2.3 Silver Nanoparticle/PLA Nanocomposites

Metal nanoparticles are also prefered for the production of polymer matrix nanocomposites because of their antibacterial, catalytic, intriguing optical and electrical properties. Due to its antibacterial activity, silver nanoparticles (Ag NP) were used in PLA matrix for food packaging applications. For example, Xu and co-workers showed that PLA fibers containing Ag NPs reduce *Staphylococcus aureus* and *Escherichia coli* microorganisms by 98.5 and 94.2 %, respectively [48]. Recently, mechanical properties of Ag NP/PLA nanocomposites were also investigated by Fortunati and co-workers. It was observed that, the increased Ag NP content improved the tensile strength and Young's modulus; however, it decreased the percent elongation at fracture [49].

2.2. Silver Nanowires

2.2.1. Polyol Synthesis of Silver Nanowires

Solution based synthesis methods were widely used in literature for the synthesis of like ceramic, metallic nanoparticles and nanowires [50]. One of this solution based synthesis methods is the "polyol process". The "polyol" term describe the high boiling point alcohol such as ethylene glycol (EG) and glycerol which is used as a solvent. Fievet and coworkers were the pioneers in this method and demonstrated the synthesis of different colloids of metals and alloys [51]. The polyol process starts with the reduction of the inorganic salt by a high melting point solvent. Then, a stabilizing agent (in most case a polymer) covers the surface of the nucleated particles and prevents possible agglomerations. Different types of nanoparticles, nanorods and nanowires with various dimensions can be produced via polyol process, because nucleation and growth steps can be easily controlled. Moreover, some metals such as nickel (Ni), cobalt (Co), lead (Pb) have low reduction potential and can only be reduced with a high boiling point solvent at high temperatures. Therefore, for some of the metals

polyol method is the only one to follow. Nanostructures of Ag were extensively investigated by Prof. Xia's group at Georgia Institute of Technology in 2002 [52]. In a parametric study, different Ag nanostructures were demonstrated by the group using EG as both the solvent and the reducing agent, PVP as the stabilizing agent and silver nitrate ($AgNO_3$) as Ag source.

In a typical synthesis, particles with different geometries, such as spherical, cubical and penta twin particles nucleate first. Once penta twin Ag particles are formed, due to energy difference between {100} and {111} planes, {111} surfaces of the particles are completely covered with PVP and fresh Ag^+ ions deposit onto the free {100} surfaces, resulting in one-dimensional anisotropic growth [53]. The schematic representations for the growth mechanism of Ag NWs from the penta twin particles is provided in Figure 2.9.

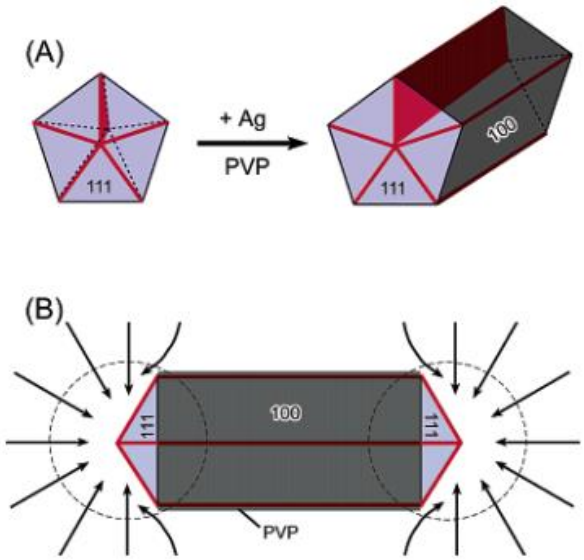

Figure 2.9. Schematic representations of (a) an individual NW growth from the penta twin particle. The tips of the NW are {111}, the side surfaces of the NW are {100} planes of FCC structure. The strong PVP interaction with {111} planes are represented with dark-gray whereas the weak interaction with {100} planes are in blue color. The red lines indicate the twin boundaries, which can act as active sides for newly reduced Ag^+ ions, (b) the diffusion of atoms to the active tips [54].

Xia and coworkers developed the salt mediated PVP assisted polyol method for the synthesis of Ag NWs between years 2002 and 2009 [52-55]. It has been shown that the existence of trace amount of salt, such as sodium chloride (NaCl), copper (II) chloride ($CuCl_2$), copper (I) chloride (CuCl) and iron nitride (FeN) effects the morphology and yield of nanostructures.

2.2.2. Silver Nanowire Reinforced Polymer Matrix Nanocomposites

First time in literature, Gelves and coworkers used Ag NWs as conductive fillers in polystyrene (PS) matrix [11]. In this paper the percolation thresholds of Ag and Cu NWs were compared. Electrodeposition technique was used for the fabrication of Ag and Cu NWs instead of polyol method. SEM and TEM images of the as synthesized Ag NWs are provided in Figure 2.10. The overall length of Ag and Cu NWs were measured as 1-2 μm.

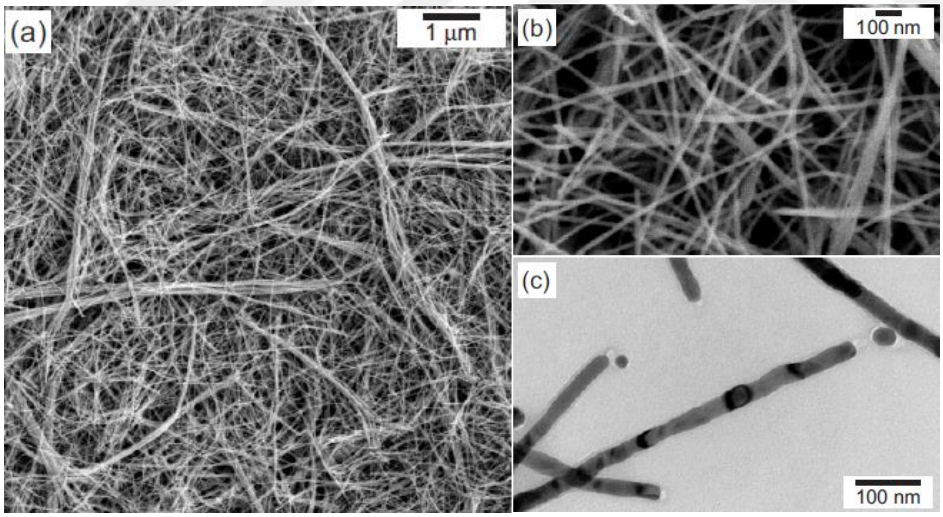

Figure 2.10. (a-b) SEM and (c) TEM images of electrodeposited Ag NWs [11].

Percolation threshold of the Ag NW/PS and Cu NW/PS nanocomposites were both measured as 0.5 vol. % from the graphs shown in Figure 2.11. Volume resistivity of Ag and Cu NW reinforced nanocomposites at the percolation threshold were 6 and 8

ohm.cm, respectively. The lower surface resistance of Ag NW/PS nanocomposites was a result of higher intrinsic conductivity and environmental stability of Ag NW compared to Cu counterparts.

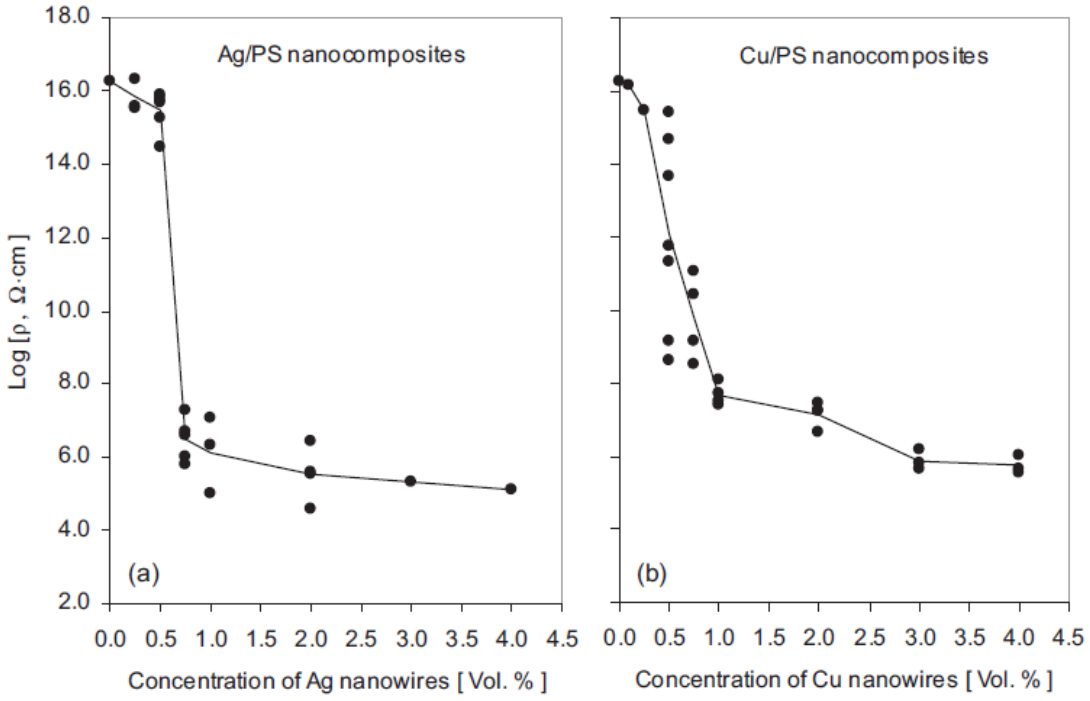

Figure 2.11. Change in volume resistivity of the nanocomposites with respect to vol. % of (a) Ag and (b) Cu NWs [11].

In another study, White et al. investigated the effect of Ag NW's aspect ratio on the percolation threshold. Electrodeposition technique was used again for the synthesis of Ag NWs with a diameter of 200 nm and different aspect ratios. Simulation results showed that the percolation threshold of the system was lower for high aspect ratio Ag NWs as expected. In another study from the same group, the temperature dependent resistive switching characteristics of Ag NWs/PS nanocomposites were investigated. In this work, two nanocomposites with different Ag NW aspect ratios were produced and their resistance with respect to temperature was monitored. These graphs are

provided in Figure 2.12 [56]. It was simply proven that Ag NW/PS matrix composites showed very promising resistive switching behavior for the memory applications

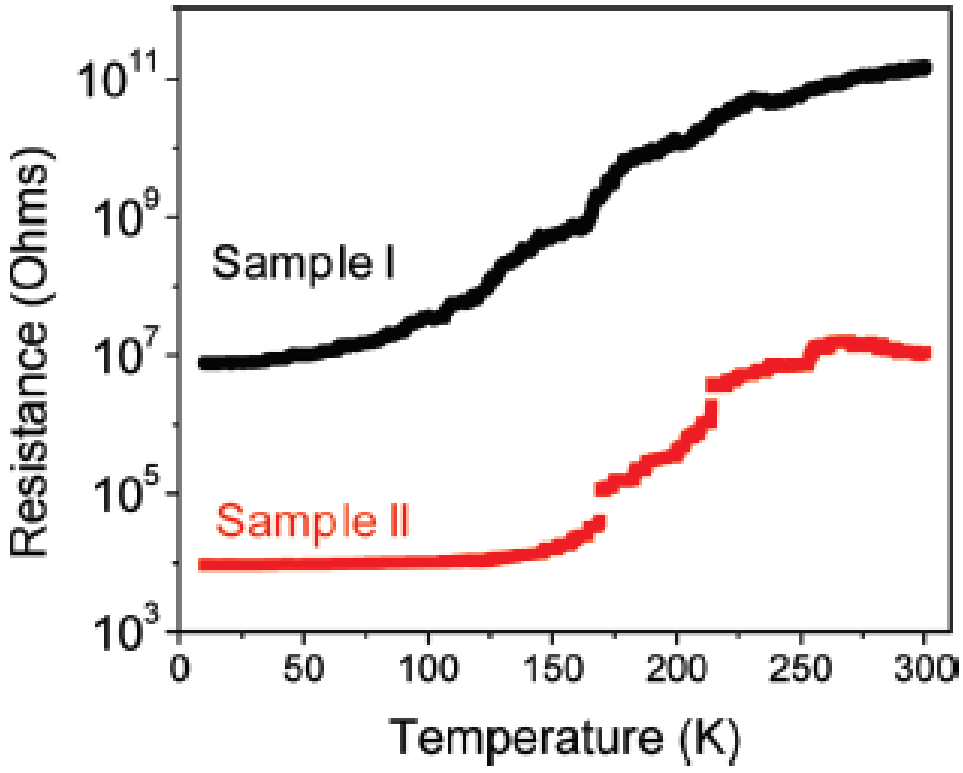

Figure 2.12: Change in resistance of Ag NW/PS nanocomposites with respect to temperature [56].

Two years later in 2012 Lonjon and coworkers compared the effects of Ag NW synthesis method on the percolation threshold of poly(vinlylidenefluoride-trifluoroethylene) (P(VDF-TrFE)) matrix composites [57]. Both electrodeposition and polyol methods were used for the production of Ag NWs. Average diameters and length of the Ag NWs produced via electrodeposition method were 200 nm and 50 microns, respectively. In this technique, an anodic alumina (AAO) template was used for the electrodeposition, which was later dissolved in sodium hydroxide (NaOH) using ultrasonication. On the other hand, the diameter and length of Ag NWs synthesized via polyol method were 100-300 nm and 20-80 microns, respectively.

SEM images of the fracture surfaces of both nanocomposites are provided in Figure 2.13. It is clear that ultrasonication process used following electrodeposition changed the straight morphology of the Ag NWs as shown in the Figure 2.13 (a). In contrast, polyol synthesized Ag NWs were straight as shown in Figure 2.13 (b).

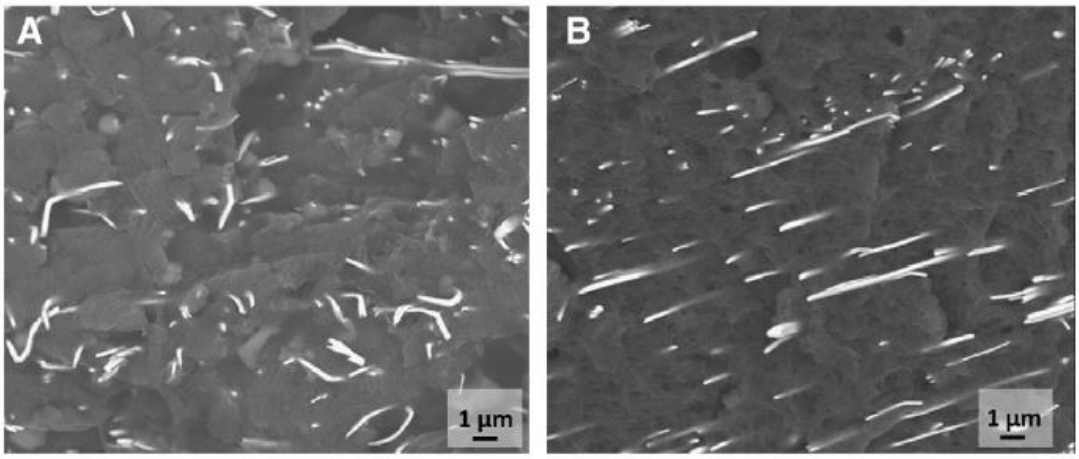

Figure 2.13. SEM images of the fractured surfaces of 3 vol. % (a) electrodeposited, and (b) polyol synthesized Ag NW/P(VDF-TrFE) nanocomposites [57].

A plot showing the electrical conductivity of the nanocomposites that Lonjon and coworkers fabricated with respect to the Ag NW content provided in Figure 2.14. Electrical conductivity of Ag NPs was also provided within the same figure. The percolation threshold of Ag NP filled composites was measured as 15 vol. %. Moreover, although the aspect ratio of Ag NWs synthesized with different methods were almost the same, different percolation thresholds were measured. Percolation threshold for electrodeposited Ag NWs was 2.2 vol. %, whereas that for polyol synthesized NWs was 0.65 vol.%. This difference was mainly due to the curved structure of the electrodeposited Ag NWs. Same research group also used polyamide 11 as a matrix material to fabricate Ag NW filled electrically conductive nanocomposites [58]. In this work solution mixing and melt mixing methods were combined for the fabrication. Melt mixing method is the most widely used composite production method. Production of homogenously dispersed, low aspect ratio particle

filled nanocomposites can be easily achieved via this method. High shear rate induced in this method may damage, the particles with high aspect ratio. On the other hand, homogeneous dispersions can easily be produced by solution mixing method; however, it is difficult to apply this process in industrial scale. Therefore, researchers firstly used solution mixing to get a homogenous dispersion resulting without any particular damage. Afterwards the nanocomposites were pelletized using an extrusion process. As a result of this combination, percolation threshold was measured as 0.59 vol. % from the fabricated nanocomposites using the plot provided in Figure 2.15. This percolation threshold value was relatively lower than the previous study of these authors, which was 0.65 vol. %.

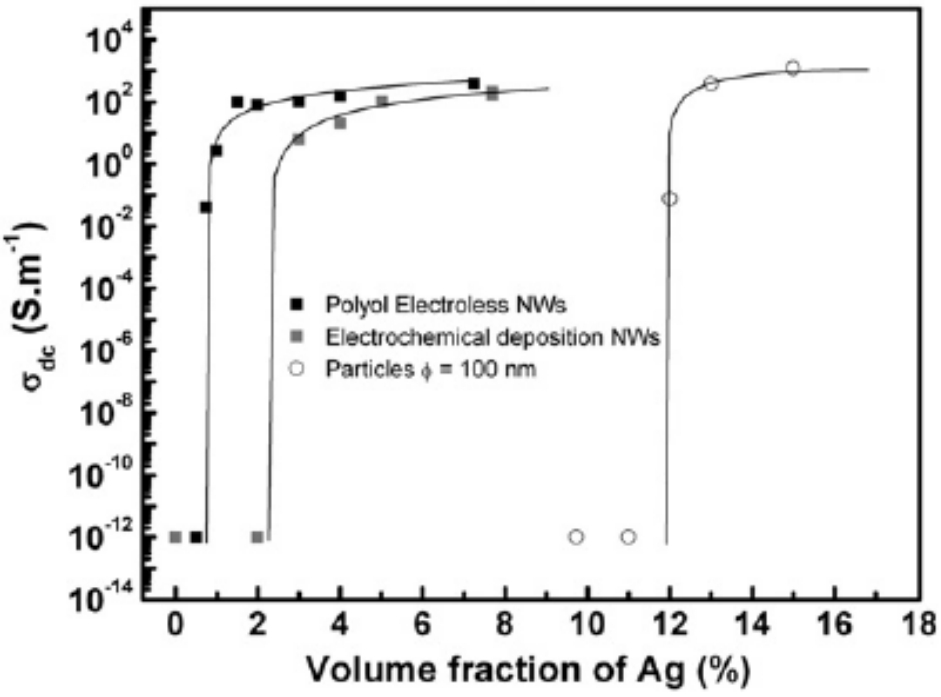

Figure 2.14. Volume electrical conductivity of both Ag NP and Ag NW filled P(VDF-TrFE) nanocomposites [57].

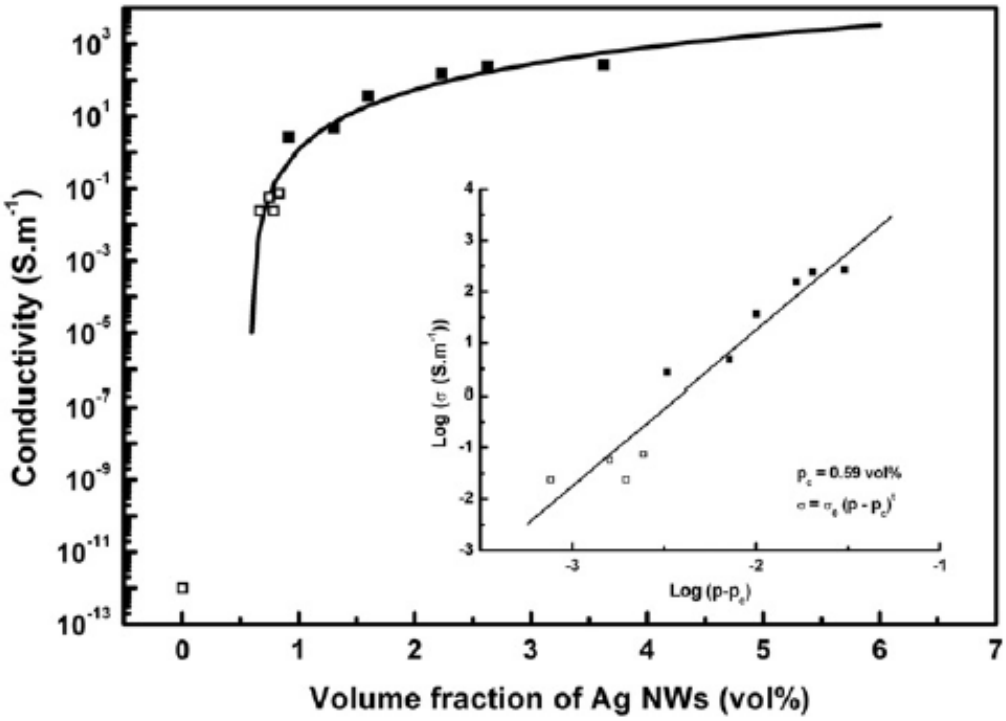

Figure 2.15. Volume electrical conductivity of Ag NW/polyamide 11 nanocomposites. Inset is the conductivity versus Ag NW volume difference in logarithmic scale [58].

These authors have also investigated the thermal properties of the nanocomposites via differential scanning calorimeter (DSC) analysis. In this analysis technique a sample and a reference is used to measure the required amount of heat to increase the temperature to a certain point. According to DSC analysis, glass transition temperature of polyamide 11 slightly decreased (by 1 ^{o}C) upon Ag NW addition as provided in Figure 2.16 (a). This slight decrease was attributed to the possible hydrogen bond formation within the matrix that stabilizes the amorphous phase. Crystallization behavior of the nanocomposites was also investigated. Surprisingly, it was found that the addition of Ag NWs did not affect the percent crystallinity of the matrix as shown in Figure 2.16 (b). This behavior was not typical for nanocomposites, but it was obvious that Ag NWs did not act as extra nucleation sites for PA11 chains.

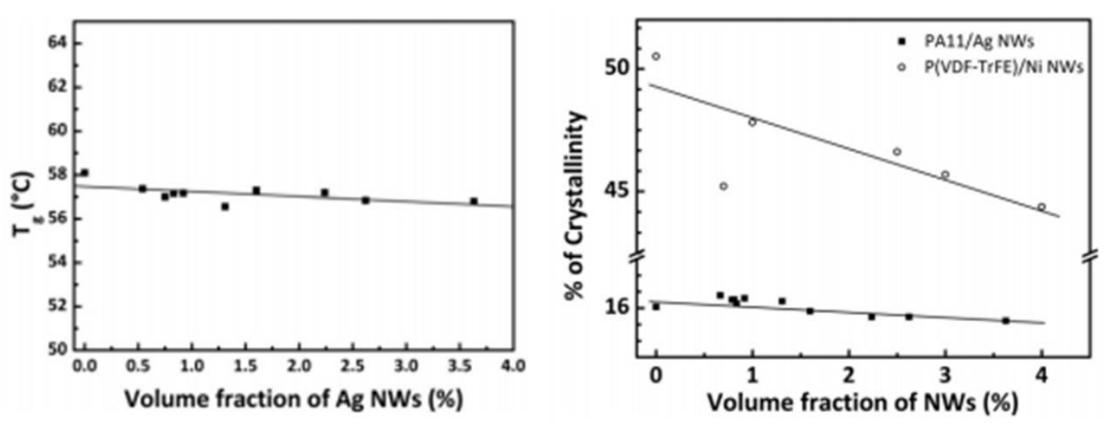

Figure 2.16. Change in (a) glass transition temperature and (b) % crystallinity with respect to Ag NW volume fraction [58].

Polycarbonate (PC) is another polymeric matrix material used with Ag NWs to produce electrically conductive nanocomposites [59]. In this work by Moreno et al., polyol synthesized Ag NWs were dispersed into tetrahydrofuran (THF) and this solution was mixed with 30 ml of the THF/PC solution. Following mixing, solution was stirred at 70 ^{o}C to evaporate the excess solvent and the obtained viscous solution was spread onto a glass substrate with a rod. Ag NWs were homogenously dispersed within the PC matrix as shown in the optical microscope and SEM images provided in Figure 2.17 (a)-(d). From these figures, it can be easily stated that Moreno and coworkers well dispersed Ag NWs within the matrix. As a results of the good dispersion, percolation threshold of the Ag NW/PC nanocomposite films were measured as 0.04 wt.%, which corresponds to 0.012 vol. %. This value is less than any other Ag NW study in the literature.

In 2014, Sureshkumar and coworkers investigated the percolation behavior and electrical conductivity of Ag NW/polystyrene (PS) nanocomposites [60]. Authors compared the latex blending and coagulated precipitation techniques in this work. In latex blending technique, polyol synthesized Ag NWs were dispersed in distilled water (DI). Then, desired amount of PS microspheres were mixed with this Ag NW solution by ultrasonication. Afterwards, the mixture was frozen with liquid nitrogen for the

removal of the aqueous remnant using freeze-drying method. Finally, the composite powders were shaped into 1-2 mm thick samples through compression. Latex blending technique is summarized and schematically represented in Figure 2.18.

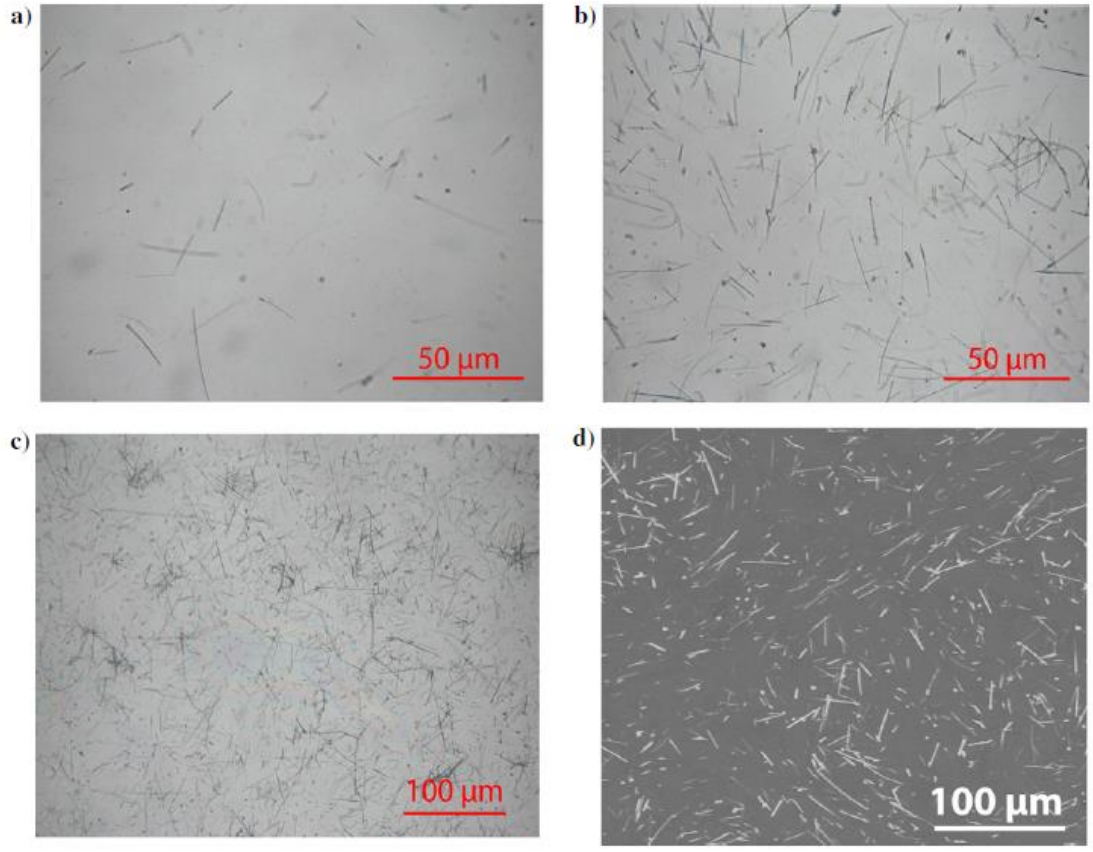

Figure 2.17. Optical microscope images of (a) 0.04 (b) 0.16 and (c) 0.64 wt. % Ag NW included PC nanocomposite films. (d) SEM image of 1.73 wt% Ag NW/PC nanocomposite film [59].

On the other hand, in coagulated precipitation technique, PS was dissolved in toluene and Ag NWs were dispersed within the same solution. Upon mixing this solution with water Ag NW/PS precipitates were collected. The collected precipitates were shaped into a disk form via compression molding. Percolation threshold of the fabricated disk shape nanocomposites were measured as 0.49 and 0.99 vol. % for latex blended and coagulated precipitates techniques, respectively. This difference between these two

methods was attributed to the better dispersion of Ag NWs within the PS matrix achieved by the latex blending technique. Consistent with the previous work the electrical conductivity of latex blended samples at 1 and 3 vol. % Ag NWs loading were 10^2 and 10^3 S/m for latex blended and coagulated precipitates techniques, respectively.

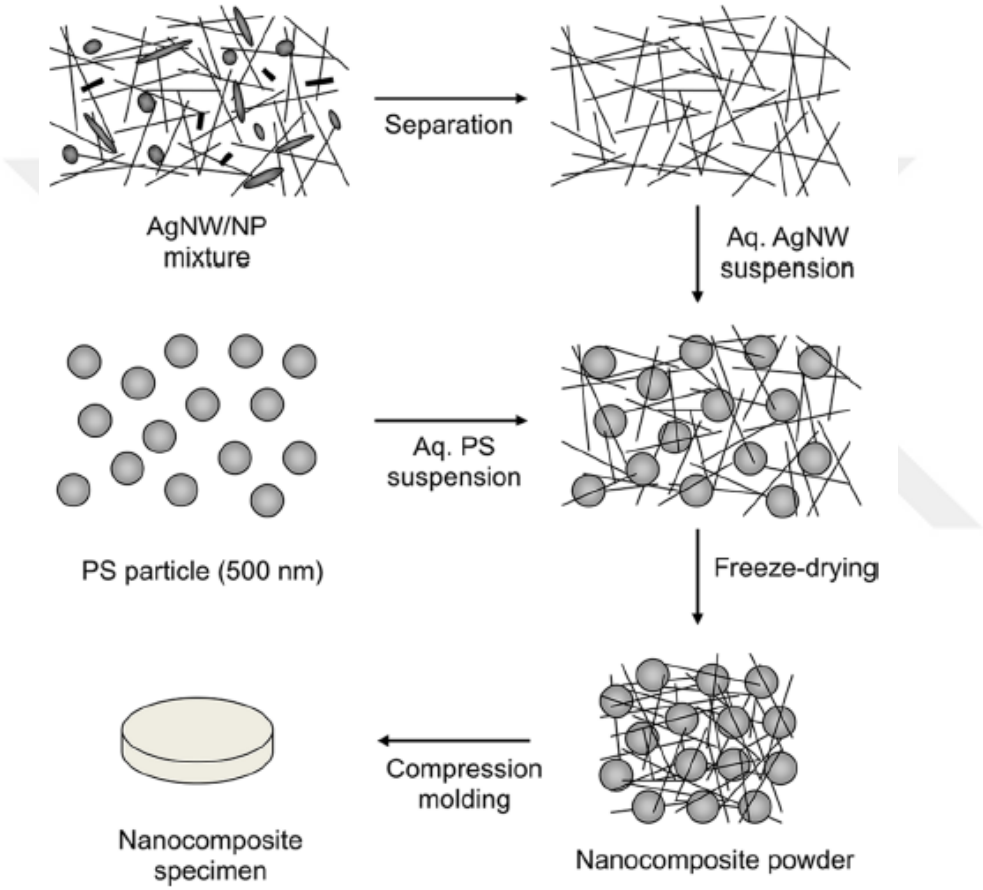

Figure 2.18. Schematic representation of the latex blending method used to produce Ag NW/PS nanocomposites [60].

Effects of hybrid structure of Ag NWs and silicon dioxide nanparticles (SiO_2 NP) on the percolation threshold were investigated by Wei and coworkers in 2015 [60]. Desired fractions of ethanolic Ag NWs and SiO_2 NPs were mixed in an ultrasonic bath, which was followed by the addition of aqueous polyurethane (PU) solution. Finally,

the solution was deposited onto office paper and dried at 60 ^{o}C for 24 hours for the formation of nanocomposites. A schematic showing the formation of nanocomposites and the interaction between Ag NWs and SiO_2 NPs is provided in Figure 2.19. According to Fourier transform infrared spectroscopy (FTIR) and X-Ray fluorescence spectroscopy (XRF) analysis, interaction between Ag NWs and SiO_2 were both van der Waals attraction and hydrogen bonding. Authors reported that the percolation threshold was dramatically decreased from 10.6 to 3.6 vol. % upon the addition of the SiO_2 NPs. This was mainly due to the improved dispersion upon modification. The Ag NW/SiO_2 NP hybrid system was also studied by another research group within epoxy matrix [61]. Authors have used Monte Carlo simulations and showed that the attractive van der Waals interactions resulted in a decrease in the depletion-induced interactions between Ag NWs, which improved the dispersion.

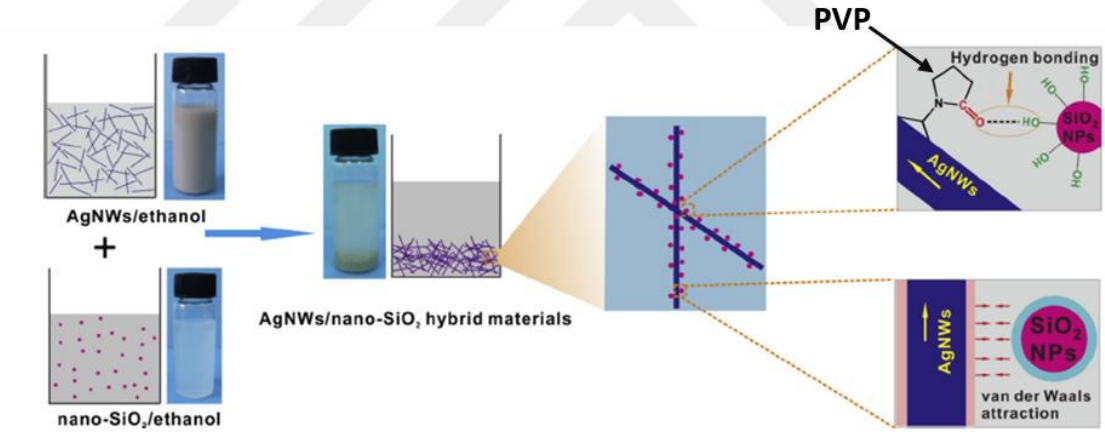

Figure 2.19. Schematic representations of Ag NWs and SiO_2 NPs interface interactions [61].

CHAPTER 3

EXPERIMENTAL DETAILS

3.1 Materials Used

3.1.1. Matrix Polymer (PLA)

L-lactic acid based polylactide (PLA) granules used in this thesis was provided by NaturePlast (PLI 003). According to the technical data sheet, the density of this PLA is 1.25 g/cm^3. Its molecular weight was measured as 980000 by Kaynak et al. [62].

3.2. Ag NW Synthesis and Nanocomposite Preparation

3.2.1. Ag NW Synthesis

Chloroform was purchased from Merck. It was utilized for the dispersion of Ag NWs and for the dissolution of PLA. All other chemicals were purchased from Sigma Aldrich and were used without further purification. Poly (vinylpyrrolidone) PVP (molecular weight=55000), ethylene glycol (EG), silver nitride ($AgNO_3$), sodium chloride (NaCl, 99.5 %) were used for the synthesis of Ag NWs. Ag NWs were synthesized according to a procedure reported by Coskun et al. [63]. For the synthesis, a 10 ml of 0.45 M EG/PVP solution was prepared and 7 mg of NaCl was added into this solution. This solution was placed into a silicon oil bath heated to 170 ^{0}C and stirred at 1000 rpm with a magnetic stirrer throughout the synthesis process. Meanwhile, a 5 ml of 0.12 M $AgNO_3$ /EG solution was added dropwise into the PVP solution at a rate of 5 ml per hour by an injection pump (Top-5300 model syringe pump). At the end of the injection process, the solution was kept at the same temperature for another 30 minutes. Following synthesis, Ag NW solution was diluted

with acetone and centrifuged at 7000 rpm for 20 minutes. Afterwards, Ag NWs were again dispersed in acetone and another centrifuge process was applied with the same parameters. Later, Ag NWs were dispersed in chloroform for further processing. Following purification, NWs were separated from syntheses by-products. This separation practiced via several simple decantation steps.

3.2.2. Preperation of the Nanocomposite Films

PLA powders were dried at 80 ^{0}C for 12 hours under vacuum. Afterwards, 1 g of PLA powder was dissolved in 10 ml of chloroform, through stirring (at 1000 rpm) at room temperature. Desired amount of Ag NWs (dispersed in chloroform) were then added to this PLA solution. Solution was mixed continuously at room temperature until it becomes a viscous liquid. Finally, the solution was doctor-bladed onto glass substrates in the form of a 20 μm thick composite film as schematically presented in Figure 3.1. To remove the solvent and entrapped bubbles from the nanocomposites, films were dried at 60 ^{0}C for 24 hours under vacuum [64]. Finally, free standing nanocomposite films were peeled off from the glass substrates and used for characterization and measurements.

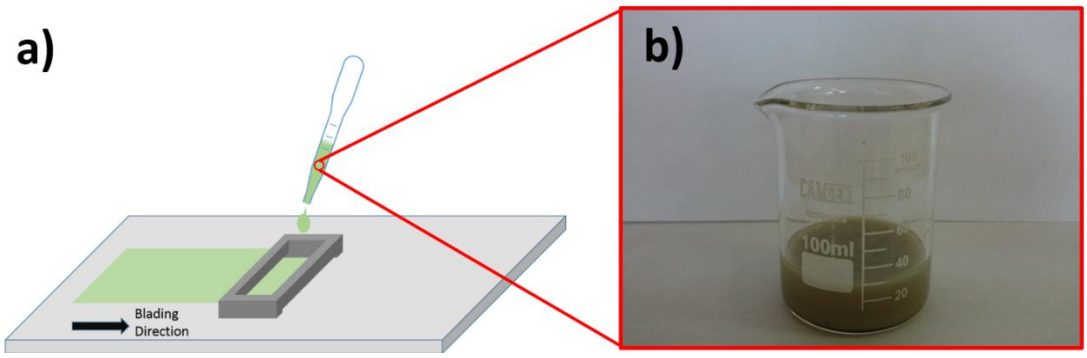

Figure 3.1. (a) Schematic presentation of the doctor blading method investigated herein this work. (b) Photograph of Ag NWs suspended in PLA/chloroform solution.

3.3. Characterization of Ag NWs and Nanocomposites Films

3.3.1. Transmittance Measurements

Ocean Optics Maya 2000 model spectrometer was used to measure the direct transmittance of the nanocomposite films within the visible range (400-700 nm).

3.3.2. Scanning Electron Microscopy (SEM) Analysis

Morphology of the nanocomposites and NWs together with the orientation of Ag NWs within the nanocomposites was characterized by scanning electron microscopy (FEI Nova Nano SEM 430). SEM was operated under an accelerating voltage of 5 kV following a thin gold layer (5-10 nm) deposition onto the samples. Since electrical conductivity measurements were made along the thickness of the nanocomposites, fracture surface of the film samples were important and was also examined via SEM. For the fracture surface analysis, nanocomposite films were immersed in liquid nitrogen (for 5 min) and then broken into pieces.

3.3.3. Thermogravimetric Analysis (TGA)

To precisely determine the Ag NW content of each nanocomposite and to investigate the thermal degradation processes of the nanocomposites, TGA analysis was performed. An Exstar SII TG/DTA 7300 system operated under nitrogen atmosphere was utilized for this purpose. Samples were analyzed in between 30 and 550 ^{0}C with a heating rate of 10 ^{0}C/min. 10 mg of neat PLA sample was also analyzed to calculate the amount of ash. Differential thermal gravimetric analysis (DTGA) was used to determine the thermal degradation temperatures of the nanocomposites.

3.3.4. Differential Scanning Calorimeter (DSC)

To investigate the crystallinity and important transition temperatures of the nanocomposites, DSC analysis was performed. An Exstar SII X-DSC 700 system was utilized and operated under nitrogen atmosphere. Firstly, to erase the thermal history, 10 mg of the sample was first heated with a heating profile from -80 to 220 ^{0}C at a

heating rate of 5 ^{0}C/min. Then the sample was cooled to -80 ^{0}C with a cooling rate of 5 ^{0}C/min. Then second heating scan was performed with the same heating profile and rate. Crystallinity percent (X_c) of the neat PLA and the matrix of the nanocomposite films were calculated using the following equation:

$$X_c = \frac{\Delta H_m - \Delta H_c}{\Delta H_m^0 \times w_{PLA}} \times 100 \quad (1)$$

,where ΔH_m is the enthalpy of melting, ΔH_c is the enthalpy of cold crystallization, ΔH_m^0 is the enthalpy of melting of 100% crystalline polymer and w_{PLA} is the weight fraction of PLA, which is equal to 93.0 J/g [65].

3.3.5. Fourier Transform-Infrared (FTIR) Spectroscopy

To investigate the possible interfacial interactions between Ag NWs and PLA, attenuated total reflectance (ATR) unit of FTIR spectrometer (Bruker ALPHA) with a resolution of 4 cm^{-1} was used within a wavenumber range of 400 - 4000 cm^{-1}.

3.3.6. Electrical Conductivity Measurements

Electrical conductivities of the nanocomposites were calculated according to the following formula:

$$\sigma = \frac{1}{R} \times \frac{t}{A} \quad (2)$$

, where σ is DC conductivity, R is resistance,A and t are the area and thickness of the samples, respectively. Resistivity of the nanocomposites were measured via Keithley 2400 SourceMeter (Keithley Instruments, INC.). A swegelok cell was used to measure the resistivity of the nanocomposite films along their thickness. Ten different spherical specimens with a radius of 1 cm were used for the measurements.

3.3.7. Tensile Test

To obtain tensile strength and elastic modulus of bare PLA and nanocomposites, tensile test was carried out according to ASTM D882-12 standard. A 100 N universal

testing machine (Zwick/Roell Z250) was used with a crosshead speed of 50 mm/min. The 20 μm thick films were cut into the form of dog bone with a gage length of 25 mm and width of 5 mm. Five specimens for each Ag NW loading was tested in parallel axis to the NW alignment direction.

CHAPTER 4

RESULTS AND DISCUSSION

4.1. SEM analysis

4.1.1. Determination of Ag NW morphology

A SEM image of purified Ag NWs is provided in Figure 4.1 (a). Average diameter and length of the Ag NWs used in this work were 60 nm and 8 μm, respectively. Detailed SEM analysis revealed the presence of a thin PVP layer on the lateral surfaces of the NW, as shown in Figure 4.1 (b). PVP was used as a stabilizing agent in the polyol synthesis of Ag NWs. Although this thin PVP layer increases the NW-NW junction resistance, it is useful to achieve stable dispersions of Ag NWs in different media like water, acetone and chloroform [66].

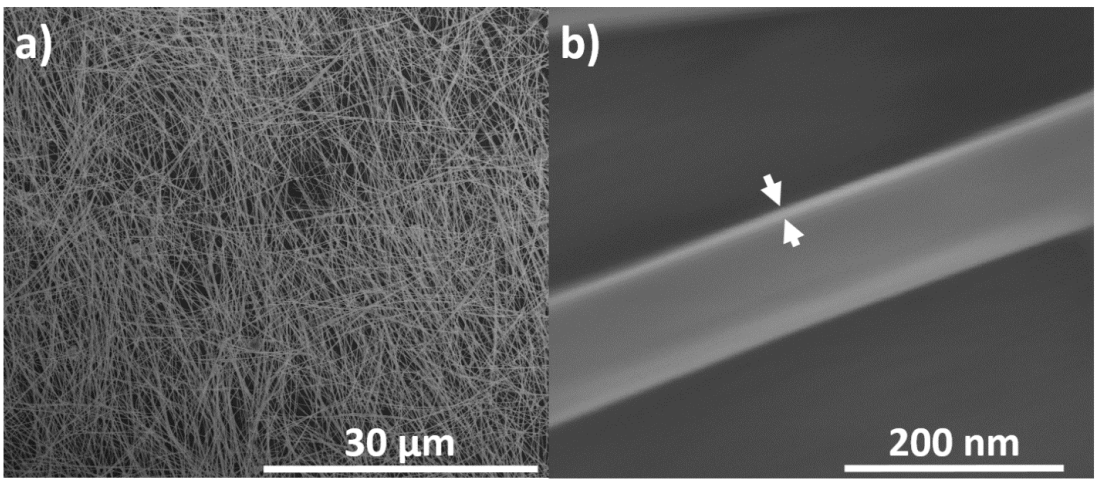

Figure 4.1. SEM images of (a) Ag NWs and (b) an individual Ag NW. Arrows point residual polymer layer on the lateral surface of the NWs.

4.1.2 Distributions of Ag NWs within PLA matrix

Figure 4.2 (a)-(c) shows the SEM images of 0.13, 0.66 and 1.74 vol.% Ag NW loaded nanocomposites, respectively. NWs showed good dispersion even at high loading levels, which was attributed to the presence of PVP on the lateral surfaces of the NWs. It is clear in terms of dispersion that the Ag NWs synthesized through polyol method is significantly better than counterparts obtained through electrodeposition [11]. A continuous network was visually observed at a Ag NW loading of 0.66 vol.% from the SEM image provided in Figure 4.2 (b). SEM image of the fracture surface of the same nanocomposite is provided in Figure 4.2 (d). Since conductivity measurements were made across the thickness of the nanocomposites, cross-sectional SEM images are crucial to understand the three dimensional percolative behavior of the NWs.

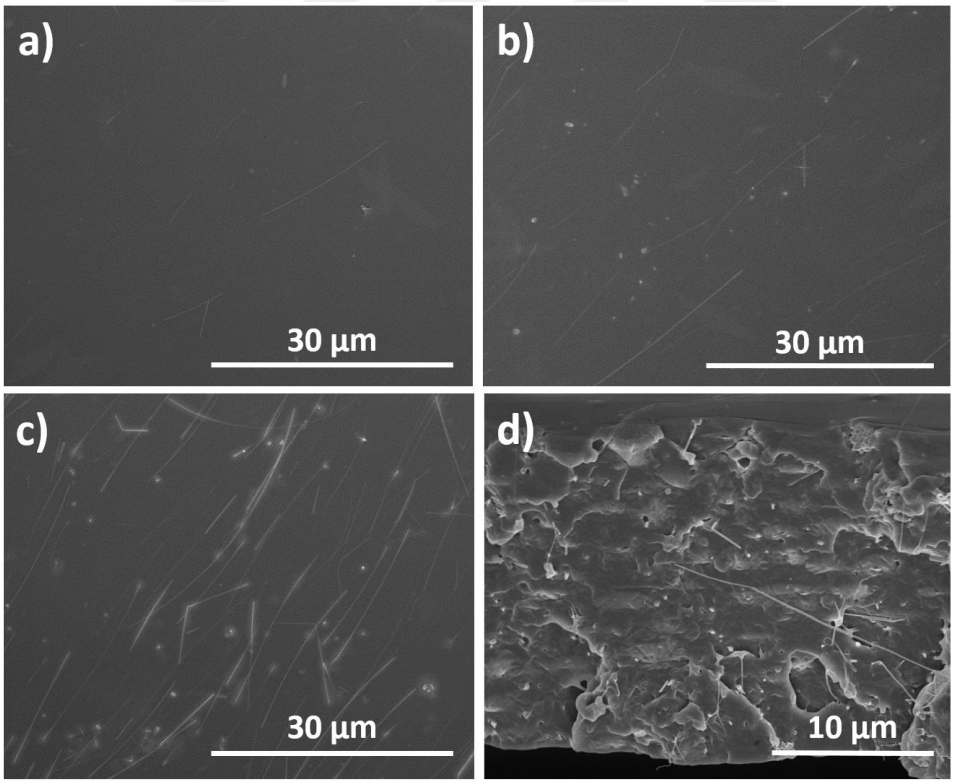

Figure 4.2. Top-view SEM images of nanocomposites with Ag NW contents of (a) 0.13, (b) 0.66, (c) 1.74 vol. %. (d) Cross-sectional SEM image of 0.66 vol.% Ag NW/PLA nanocomposite.

4.1.3. Alignment of Ag NWs within PLA Matrix

It is known that the nanofillers align within the blading direction during doctor blading due to the applied shear force [67,68]. Accordingly, in our case, as it can be seen from the SEM images (Figure 4.2 (a), (b) and (c)), Ag NWs were aligned parallel to the blading direction. The degree of alignment was simply calculated via the procedure described by Park et.al [67]. The angle between NWs and blading direction is estimated from the SEM images as show in Figure 4.3 (a). Basically, direction of an individual NW was set as a vector and the angle between blading direction and NW direction was measured. For each sample, 100 different Ag NWs were taken into consideration and an average alignment angle was calculated. [$Cos^2(\theta)$] is defined as the degree of Ag NWs alignment, which is supposed to be equal to 1 for perfect alignment, while 1/3 for random orientation. Change in [$Cos^2(\theta)$] with respect to Ag NW content is provided in Figure 4.3 (b). An average [$Cos^2(\theta)$] value of 0.88 was obtained for all Ag NW loadings. The amount of Ag NW loading within the nanocomposites did not affect the alignment of NW. This situation is in contrast with the CNT alignment within the nanocomposites [67, 68]. This difference is due to the fact that the Ag NWs were not agglomerated within the matrix.

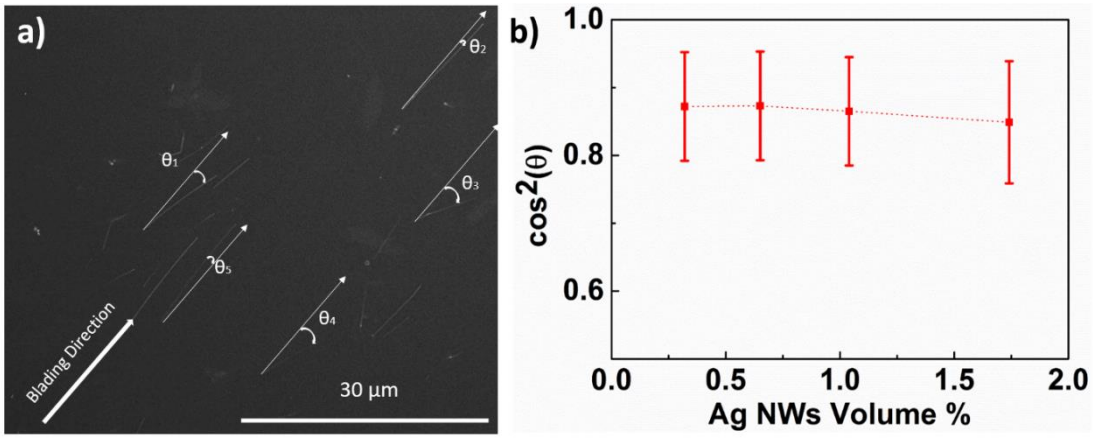

Figure 4.3. (a) SEM image of 0.66 vol.% Ag NW/PLA nanocomposite film showing the angle between NWs and the blading direction. (b) **[**$Cos^2(\theta)$] values of nanocomposites with different Ag NW loading. Lines are for visual aid.

4.2. Thermal Properties

4.2.1. Thermogravimetric Analysis (TGA)

TGA results between room temperature and 550 ^{0}C are provided in Figure 4.4 (a). Weight of the Ag NWs were measured using a micro balance prior to the fabrication of the nanocomposites. The weight of the NWs within the nanocomposites was also confirmed by TGA analysis. Almost the same values within an error margin of 5% was obtained from the TGA analysis showing consistency in our experiments. Slight mass loss from TGA curves, around 100 ^{0}C was attributed to the loss of absorbed water in PLA. Effects of Ag NWs on the thermal degradation behavior of the nanocomposites can be easily seen within DTGA curves provided in Figure 4.4 (a). Thermal degradation temperatures along with the enthalpy values and percent crystallinity of the nanocomposites are tabulated and provided in Table 4.1. The degradation temperature is almost unchanged with the addition of NWs. One of the reasons for this behavior is the lack of chemical interaction between PLA and Ag NWs. Before PLA starts to degrade, surface interactions might get lost between PLA and Ag NWs. SEM analysis was also performed on the TGA residue and the obtained micrograph is provided in Figure 4.4 (b). Although bare Ag NWs are not stable at temperatures higher than 300 ^{0}C [69, 70], most of the Ag NWs remained intact within the nanocomposites as evidenced in the figure. The stability of the NWs was attributed to the protective nature of the polymeric matrix at high temperatures (500 ^{0}C in this case) for a limited amount of time.

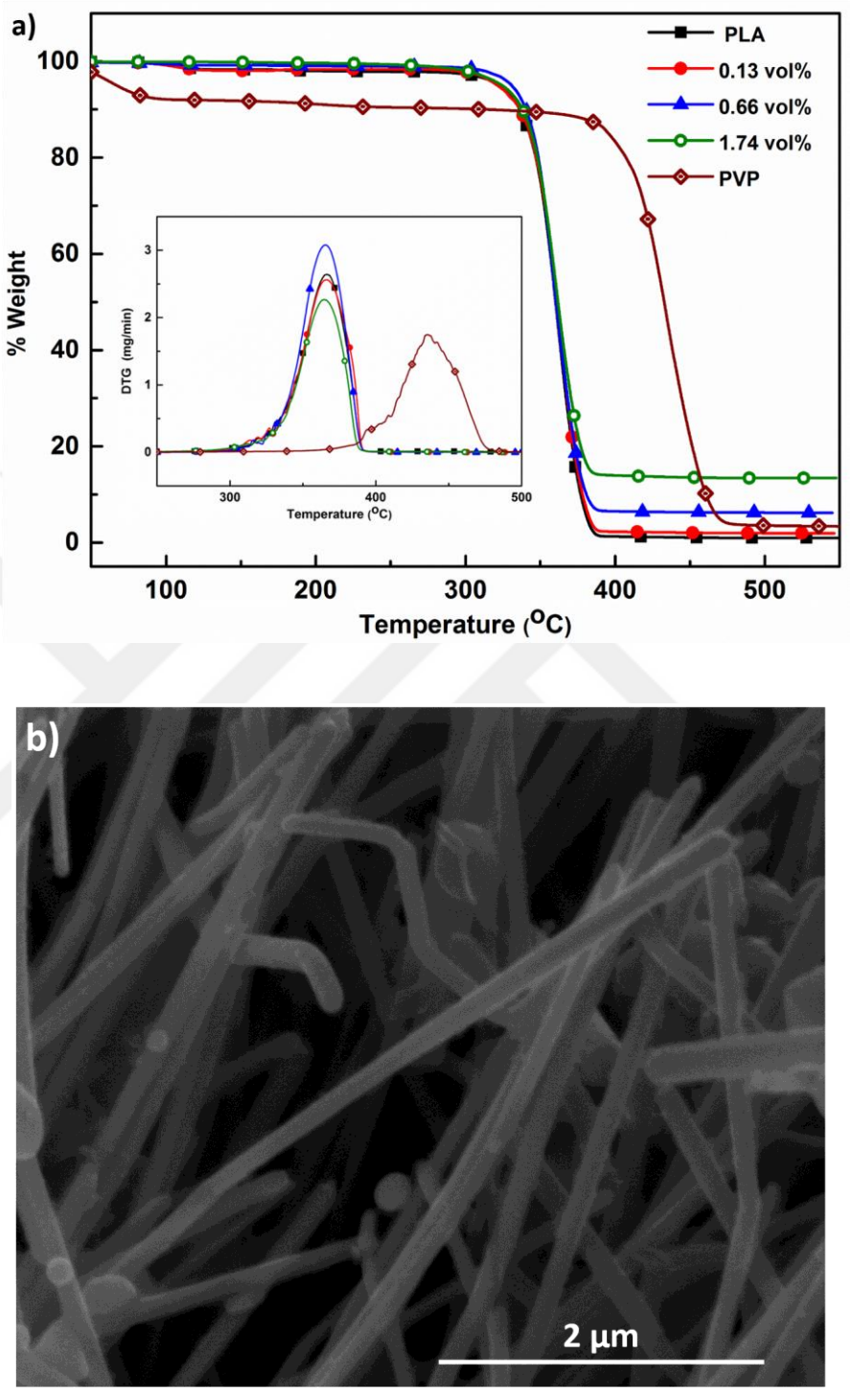

Figure 4.4. (a) Thermalgravimetric analysis of neat PLA and fabricated Ag NW/PLA nanocomposites, inset shows DTGA curves, b) SEM image of the TGA residue.

4.2.2. Differential Scanning Calorimeter (DSC)

DSC curves of neat PLA and fabricated nanocomposites are provided in Figure 4.5 (a). After erasing the thermal history, the second heating scan was recorded. Glass transition temperature T_g, cold crystallization T_c, and melting temperature T_m were measured as 62, 98, 168 ^{0}C, respectively. These transition temperatures were almost unchanged upon the addition of Ag NWs as indicated with dashed lines on Figure 4.5 (a). This behavior is consistent with the study of Lonjon et.al., where transition temperatures for PEEK were found to be unaffected with the addition of Ag NWs [12]. Crystallinity percent of neat PLA and nanocomposites are provided in Figure 4.5 (b). Crystallinity percent of neat PLA was calculated as 15 % and it was found to increase with increasing Ag NW content. This was due to Ag NWs acting as extra nucleation sites for heterogeneous nucleation. This phenomenon is quite typical for nano sized filler addition. For example, Papageorgiou and coworkers examined the effect of filler type on the crystallization behavior of PLA matrix nanocomposites. In their work, nanosized SiO_2, montmorillonite (MMT) and multiwalled carbon nanotubes (MWCNTS) were used as fillers. Activation energy for crystallization was found to be lower after SiO_2 and MWCNT additions, which also increased the percent crystallinity.

Table 4.1. Parameters determined from TGA and DSC analysis.

Ag NW content (volume %)	Degradation and Transition Temperatures (°C)				% Crystallinity (X_C)
	T_d	**T_g**	**T_c**	**T_m**	
Bare PLA	366	62	98	168	15.23±1.3
0.12	365	62	98	169	17.63±0.9
0.66	363	62	98	168	22.58±1.9
1.74	365	62	99	169	27.30±2.1

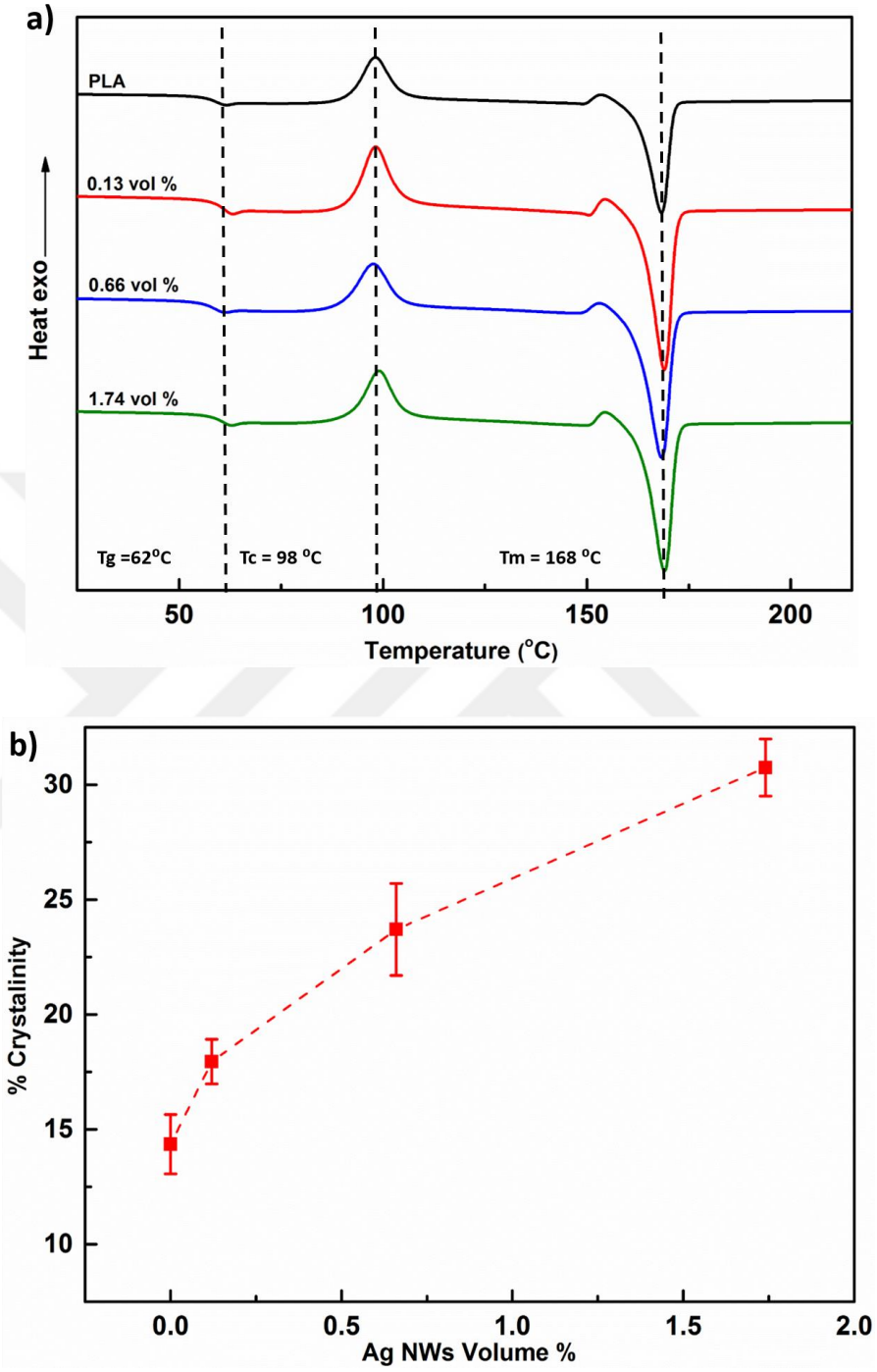

Figure 4.5. (a) Second heating DSC thermograms of bare PLA and fabricated nanocomposites, (b) percent crystallinity of PLA and fabricated nanocomposites. Lines are for visual aid.

4.3. Interfacial Interaction Between Ag NWs and PLA

FTIR spectrum of the fabricated Ag NWs/PLA nanocomposite is provided in Figure 4.6 (for 1.74 vol.% Ag NWs). Spectra for neat PLA and Ag NWs are also provided within the same figure for comparison. IR bands of PLA and Ag NWs/PLA nanocomposites are summarized and compared to literature values in Table 4.2 [62, 71-73]. Distinctive IR bands for PLA are obtained at 869 cm^{-1} (C-C stretching vibration), 1079 cm^{-1} and 1181 cm^{-1} (C-O-C asymmetric and symmetric), 1360 cm^{-1} (C-H symmetric bending), 1454 cm^{-1} (-CH_3 asymmetric bending), 1748 cm^{-1} (C=O). The peaks at 2944 cm^{-1} and 3002 cm^{-1} correspond to C-H symmetric and asymmetric stretching vibrations, respectively. IR bands for the fabricated Ag NWs /PLA nanocomposites are the same for C-C stretching, C-O-C asymmetric and symmetric stretching, C-H symmetric bending and –CH_3 asymmetric bending vibrations. There occurred an extra IR band at 2853 cm^{-1}, which indicated the existence of PVP [38]. Same band is also observed within the Ag NWs spectra, due to presence of a PVP layer. Although, a small change is observed for the nanocomposite at C=O and C-H asymmetric stretching modes (respectively from 1748 cm^{-1} to 1750 cm^{-1} and 3002 cm^{-1} to 2996 cm^{-1}) it is within the error range of the spectrometer. C-H symmetric stretching mode is found to shift from 2944 cm^{-1} to 2924 cm^{-1}. This shift is attributed to the chemical interactions between PVP and PLA.

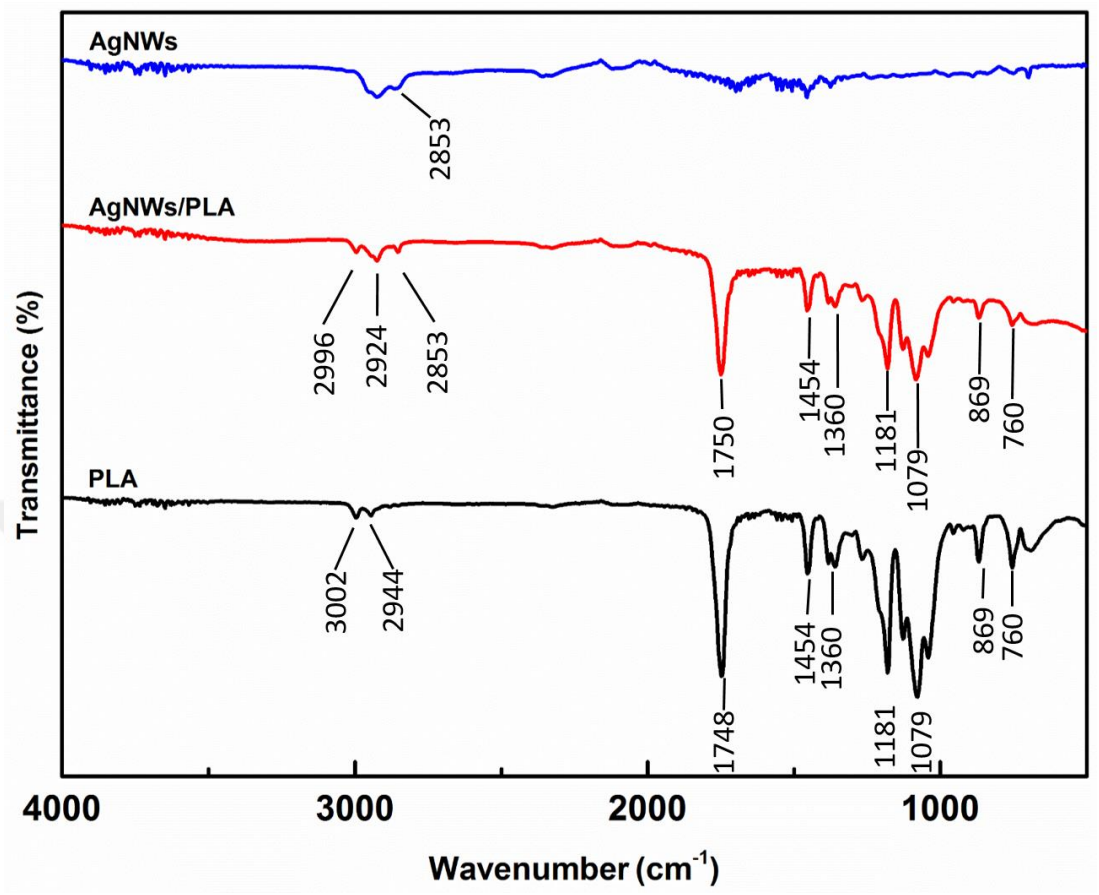

Figure 4.6. FTIR spectrum of the bare PLA, Ag NWs and 1.75 vol.% Ag NW/PLA nanocomposites.

Table 4.2. Positions and assignments of distinctive IR bands of PLA, Ag NWs and fabricated nanocomposites.

Materials	Positions (cm^{-1}) (In this work)	Position (cm^{-1}) (In literature) [36,37,38]	Assignments
PLA	869	868	C-C stretching
	1079	1093	C-O-C asymmetric stretching
	1181	1180	C-O-C symmetric stretching
	1360	1382	C-H symmetric bending
	1454	1456	$-CH_3$ asymmetric bending
	1748	1756	C=O stretching
	2944	2944	C-H symmetric stretching
	3002	2997	C-H asymmetric stretching
Ag NWs	2853	2873	C-H stretch of PVP
AgNWs/ PLA	869		C-C stretching
	1079		C-O-C asymmetric stretching
	1181		C-O-C symmetric stretching
	1360		C-H symmetric bending
	1454		$-CH_3$ asymmetric bending
	1750		C=O stretching
	2853		C-H symmetric stretching
	2924		C-H asymmetric stretching
	2996		C-H asymmetric stretching

4.4. Electrical Conductivity

Percolation threshold for three dimensional systems, which is directly related with the aspect ratio and alignment of the fillers, can be estimated by a well-known volume excluded model developed by Balberg et. al [74, 75]. Critical excluded volume for 3D system is:

$$V_{ex}^{cr} = \frac{L}{r} V_{NW} N_c = \frac{L}{r} f_c \quad (3)$$

, where L is the length of the fillers, r is the radius of the fillers V_{NW} is the volume of filler, N_c is the critical concentration of fillers, f_c is the critical volume fraction of fillers. Critical excluded volume for parallel alignment is calculated as 2.8 [75]. The aspect ratio of Ag NWs used in this study was within the range of 33 and 500. Therefore, calculated critical volume percent was within the range of 0.56 and 8.4. Electrical conductivity of the fabricated Ag NW/PLA nanocomposite films as a function of Ag NW volume fraction is provided in Figure 4.7. Although a conductive network is visually observed at a volume fraction of 0.66% via SEM analysis, percolation threshold is measured to be 0.13 vol.% for our system. The percolation threshold is not within the theoretical range, because there are NWs within the nanocomposites that are, longer than the film thickness (20 μm). As a result, our system might be out of boundary conditions of the volume excluded model. Conductivity of the nanocomposite with a Ag NW loading of 0.13 vol.% is measured as 5×10^{-4} S/m. Obtained maximum conductivity is 27 S/m, which correspond to a Ag NW loading of 1.74 vol.%. Electrical conductivity of the neat PLA is reported as 2×10^{-17} S/m in literature [76]. A conductivity change within 18 orders of magnitude is obtained for the fabricated samples. Conductivity at 1.74 vol. % is an order of magnitude lower than those reported in the literature for the same NW content. For example, conductivity of Ag NW/poly (ether ketone ketone) at the same Ag NW content was measured around 100 S/m by Lonjon et. al [12]. It is attributed to the alignment of Ag NWs within the PLA matrix. It is known that up to a certain degree of alignment,

conductivity of the nanocomposites increases since conductive path becomes shorter. However, after a critical degree of alignment, conductivity decreases; due to, a decrease in the number of alternative conducting pathways. This increases the equivalent resistance of the system [77]. Insulator-conductor behavior can be described by a power law as stated by Kirkpatrick [78]:

$$\sigma_{dc} = \sigma_0 (p - p_c)^t \tag{4}$$

, where σ_{dc} is the conductivity of the whole system, σ_0 is the conductivity of filler, p is the volume fraction of the filler, p_c is the volume fraction of the filler at percolation threshold and t is the critical exponent. For three-dimensional systems the critical exponent t is between 1.6 and 2 [4]. As discussed by Li et.al., t deviates to 1 when filler resistance is higher than the junction resistance. On the other hand, when junction resistance is higher than the filler resistance, t deviates to 2. Moreover, it was also indicated that the critical exponent can deviate to values higher than 2 if the conductivity is dominated by the tunneling resistance [79]. For our system, critical exponent upon best fit was found as $t = 2.87 \pm 0.09$. This value is higher than the universal range. It should be noted that our system is junction limited. For Ag NWs, Bellew et.al. measured a junction resistance of 500 ohms, which is a lot higher than the individual nanowire resistance [80]. It is thus clear that the conductivity of network of Ag NWs would be junction resistance dominated. In addition, in our case, a 2-3 nm thick PVP layer would dictate tunneling even if there is direct contact between the NWs. Therefore, we obtained a high critical exponent. Moreover, it should be noted that the power law is valid for random NW orientation. However as discussed before, Ag NWs are highly oriented within the fabricated nanocomposites. In addition, presence of aggregates also increases the t value. When we extrapolate the power law equation, conductivity of Ag NWs was calculated as $10^{6.74 \pm 0.27}$ S/m, which is lower than the conductivity of bulk Ag yet it is consistent with the Ag NW/polymer matrix conductive composites in literature [12].

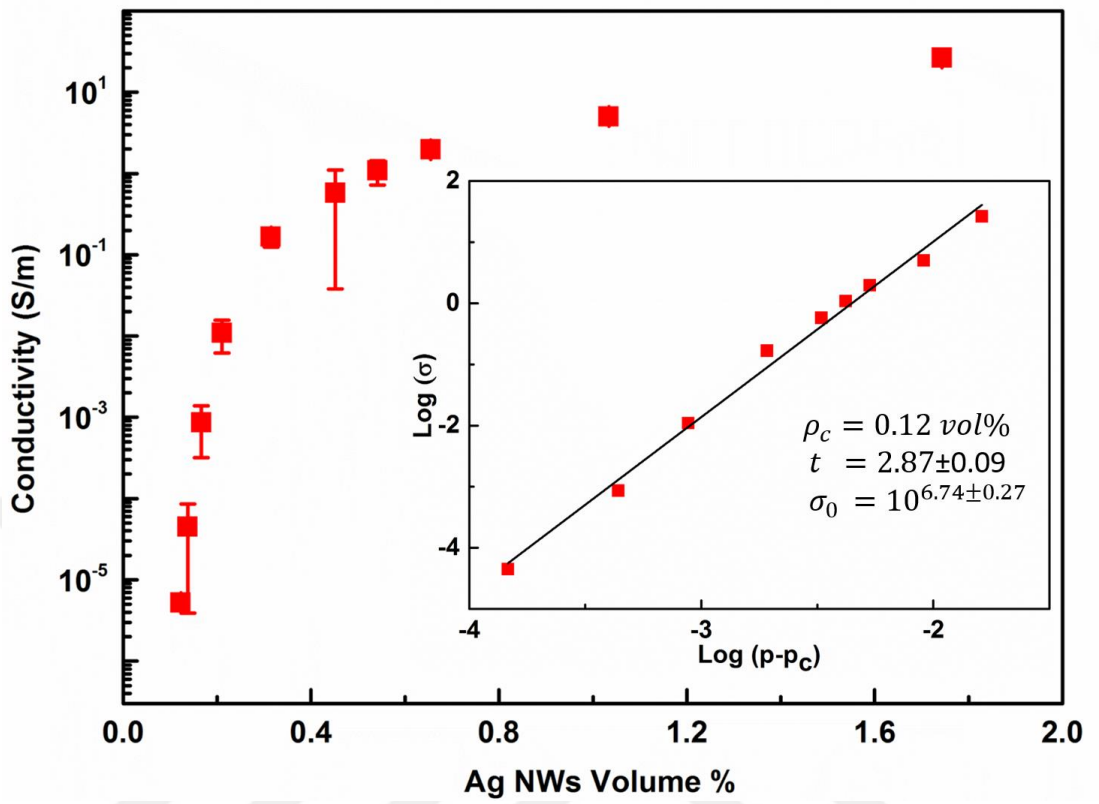

Figure 4.7 Conductivity of the fabricated Ag NW/PLA nanocomposites with respect to the Ag NW content.

4.5. Mechanical Performance

Representative tensile stress and strain curves for bare PLA and Ag NW/PLA nanocomposites are provided in Figure 4.8 (a). Tensile test is applied parallel to the blading direction. Tensile strength significantly increased up to a Ag NW loading of 0.18 vol.%. Mechanical performance is started to decrease at a Ag NW loading of 0.24 vol.%. Tensile strength values are 44, 53, 62, 59 and 56 MPa for bare PLA and nanocomposites with Ag NW contents of 0.06, 0.12, 0.18 and 0.24 vol.%, respectively. For these samples, corresponding elastic moduli are 2284, 2690, 2953, 3048 and 2750 MPa as shown in Figure 4.8 (b), respectively. The increase in mechanical performance is attributed to the successful load transfer from matrix to Ag NWs. The decrease in mechanical properties above a Ag NW content of 0.24 vol % is attributed to a decrease

in the interfacial interactions between the matrix and fillers. Higher Ag NW content necessitates the use of more chloroform to obtain uniform Ag NW dispersion. Therefore, PVP layer on the lateral surfaces of Ag NWs might get removed by this excess chloroform use, which results in a reduction of interfacial interactions. SEM image from the fracture surface of 0.24 vol % Ag NW/PLA nanocomposite film is provided in Figure 4.8 (c). Solid arrows indicate the positions of pulled out Ag NWs as a result of lack of interfacial interactions. It can be clearly seen from Figure 4.8 (b), that the standard deviations are quite high. This can be attributed to the solution casting method. Since solution casting is a pressureless method, it is impossible to completely get rid of the bubbles. In Figure 4.8 (c) dashed arrows show the bubbles within the structure.

Mechanical properties of PLA matrix nanocomposites depend on different parameters. First of all, grade of PLA directly affects the mechanical performance. It should be noted that, different PLA producers have different synthesis routes which effect the molecular weight of PLA as well as its mechanical performance. Secondly, production method also affects final properties of the nanocomposites as stated above. A small comparison list is provided in Table 4.3 for different cases [18, 81-88]. However, mechanical properties of CNT/PLA nanocomposite films reported by Yoon and coworkers is the closest study in our work. Since the initial mechanical properties of PLA and type of the nanocomposite production are very close in our case. Tensile strength enhancement of Ag NW/PLA nanocomposite films was (41%) slightly lower than the CNT/PLA nanocomposite films (47%). On the other hand, elastic modulus enhancement (34%) is slightly higher than the CNT/PLA nanocomposite films (32 %).

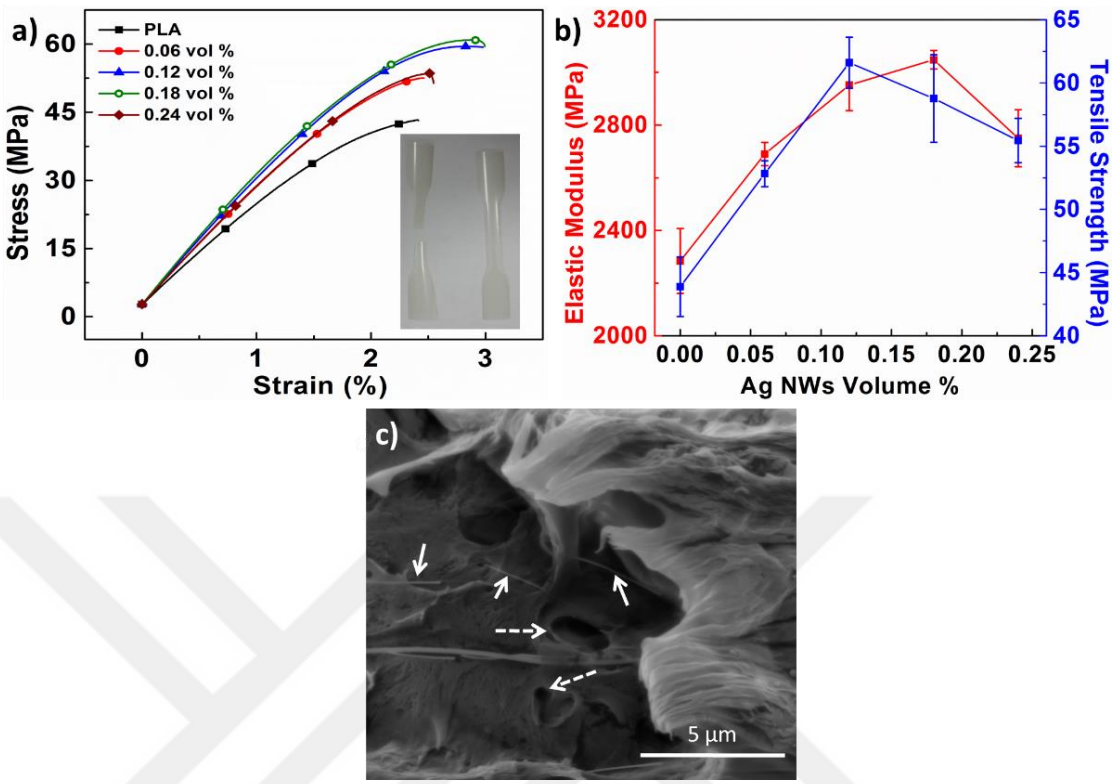

Figure 4.8: (a) Representative stress-strain curves of bare PLA and Ag NW/PLA nanocomposites. (b) Effects of Ag NW content on elastic modulus and tensile strength of the nanocomposites. (c) Cross-sectional SEM fractograph of 0.24 vol.% Ag NW/PLA nanocomposite.

Table 4.3: Mechanical performance comparison list of PLA matrix nanocomposites.

			Tensile Strength (MPa)			Elastic Modulus (MPa)			
PLA Supplier	**Additive**	**Type**	**PLA**	**Nanocomposite**	**Enhancement**	**PLA**	**Nanocomposite**	**Enhancement**	**Ref**
Biomer L9000	Nanoclay	Films	50	40	-20 %	–	–	–	18
Nature Works 4032D	Halloysite	Films	50	48	-4 %	1500	1770	18 %	81
Nature Works 3051D	Silver Nanoparticle	Films	54	31	-42 %	2400	2520	5 %	82
Cargill Dow	Clay	Films	34	32	-6 %	1406	1884	34 %	83
Nature Works	CNC	Mats	1.25	6.5	520 %	10	125	1250 %	84
Nature Works 4032D	CNT	Films	49	72	47 %	1928	253441	32 %	85
Nature Works 2002D	Graphene	Films	13	30	130 %	380	850	124 %	86
Nature Plats PLI 003	Halloysite Nanotube	Bulk	64	71	11 %	3720	4210	13 %	87
Shenzhen Bright China ESUN	Celluso Nanofiber	Bulk	59	71	20 %	2900	3600	24 %	88
Nature Plast PLI 003	Silver Nanowire	Film	44	62	41 %	2284	3048	34 %	This Work

CHAPTER 5

CONCLUSIONS AND FUTURE RECOMMENDATIONS

5.1. Conclusions

The effect of Ag NWs on the electrical, mechanical and thermal properties of 20 μm thick PLA nanocomposite films were investigated. Ag NWs were found to be highly aligned within the PLA matrix as a result of the shear induced by the blading method. It was observed that Ag NWs have almost perfect alignment (parallel to each other) even at high filler contents. TG and DSC analysis revealed that Ag NWs have no influence on the degradation and transition temperatures of PLA. Thermal degradation temperatures of both bare PLA and Ag NW/PLA nanocomposites were 365 ^{o}C. Glass transition, crystallization and melting temperatures were also unchanged which were 68, 98, 168 ^{o}C, respectively. Moreover, a remarkable increase in the percent crystallinity was obtained with the addition of Ag NWs. After 1.74 vol. % Ag NW addition, percent crystallinity were increased by 80%. Dispersion of Ag NWs within the PLA matrix was quite effective, attributed to the presence of residual PVP layer on the lateral surfaces of the NWs. Onset of the long-range connectivity known as percolation threshold was determined as 0.13 vol.%. Highest conductivity of 27 S/m was obtained for the nanocomposites with a Ag NW content of 1.74 vol.%. Moreover, mechanical properties of PLA were found to increase remarkably upon Ag NW addition. Both tensile strength and elastic modulus increased by 34% with only 0.18 vol.% NW addition. As a result of this study, it is shown that Ag NW/PLA nanocomposites have significant potential for different applications like electrostatic

packaging and electromagnetic shielding. Moreover, further increase in the mechanical performance of the nanocomposites would open new avenues in their use, such as food packaging.

5.2. Future Recommendations

In this thesis, the effect of polyol sythesized Ag NW content on the electrical, mechanical and thermal properties of PLA were investigated. Solution casting method was prefered to fabricate nanocomposite films since it is a simple and solution based route for laboratory use. However, in order to mass produce Ag NW/PLA nanocomposites, different production routes must be investigated such as injection molding. This would also allow the production of nanocomposites in bulk form rather than 20 μm thick films as investigated in this thesis.

As discussed in the previous chapters for the case of SiO_2 NPs, different nanostructured additives can be used to improve the dispersion of Ag NWs within the polymer matrix. In addition to this, surface modification method can be investigated. For example, silane modifications were widely demonstrated for the surface modification of various nanoparticles; however, it is not investigated for Ag NWs yet.

PLA is one of the most suitable and widely used polymer inks for 3D printers. Therefore, the conductive Ag NW/PLA nanocomposites can also be applied as conductive inks for conventional 3D printers for different purposes like capacitive sensors and supercacitor electrodes.

High antibacterial activity of Ag has been known for a long time and it has been widely used for this purpose. Nano structures of Ag have also been investigated in the literature. However; antibacterial activity of Ag NW shas not been investigated within a polymer matrix. Especially antibacterial PLA matrix nanocomposites have a good potential to be used in food packaging. Moreover, antibacterial 3D printer inks will undoubtedly would also create different potential applications.

REFERENCES

(1) B.L Lee. Electrically conductive polymer composites and blends, Polym. Eng. Sci., 5, 1992, 36-42.

(2) C.L. Hsang, L. Pang, M.C. Chen, P.Y. Huang, C. Kim, J.C. Ho and C.C. Lee. Silver nanowire-polymer composites electrode for high performance solution-processed thin-film transistors, Org. Electron., 13, 2012, 1881-1886.

(3) S. Choi, J. Park, W. Hyun, J. Kim, J. Kim, Y.B. Lee, C. Song, H.J. Hwang, J.H. Kim, T. Hyeon and D.H. Kim. Stretchable heater using ligand-exchanged silver nanowire nanocomposite for wearable articular thermotherapy, ACS Nano, 9, 2015, 6626-6633.

(4) D. Stauffer and A. Aharony. Introduction to percolation theory, revised second ed. Taylor & Francis, London, 1994.

(5) D.I Tee, M. Mariatti, A. Azizan, C.H. See and K.F. Chong. Effect of silane-based coupling agent on the properties of silver nanoparticles filled epoxy composites, Compos. Sci. and Technol., 67, 2007, 2584-2591.

(6) F. Gubbels, R. Jerome, Ph. Teyssie, E. Vanlathem, R. Deltour, A. Calderone, V. Parente and J.L. Bredas. Selective localization of carbon black in immiscible polymer blends: A useful tool to design electrical conductive composites, Macromolecules, 27, 1994, 1972-1974.

(7) I.W. Sadie, R.M. Motiso, P.M. Vora, D. Jahnke, S. Hsu, J.M. Kikkawa, J. Li, J.E. Fisher and K.I. Winey. Electrical percolation behavior in silver nanowire polystyrene composites: Simulation and experiment, Adv. Funct. Mater., 20, 2010, 2709-2716.

(8) J.K.W. Sandler, J.E. Kirk, I.A. Kinloch, M.S.P. Shaffer and A.H. Windle. Ultra-low electrical percolation threshold in carabon nanotube epoxy composites, Polymer, 44 2003, 5893-5899.

(9) G.A. Gelves, U. Sundararaj and J.A. Haber. Electrostatically dissipative polystyrene nanocomposites containing copper nanowires, Macromol. Rapid Commun., 26, 2005, 1677-1681.

(10) A. Lonjon, P. Demont, E. Dantras and C. Lacabanne. Mechanical improvenment of P(VDS-TrFE)/nickel nanovires conductive nanocomposites: Influence of particles aspect ratio, J. Non-Cryst. Solids, 358, 2011, 236-240.

(11) G.A. Gelves, B. Lin, U. Sundararaj and J.A. Haber. Low electrical percolation threshold silver and copper nanowires in polystyrene composites, Adv. Funct. Mater., 16, 2006, 2423-2430.

(12) L.Q. Cortes, A. Lonjon, E. Dantras and C. Lacabanne. High-performance thermoplastic composites poly (ether ketone ketone//silver nanowires: Morphological, mechanical, electrical properties, J.Non-Cryst.Solids, 391, 2014, 106-111.

(13) Y.H. Yu, C.C.M. Ma, S.M. Yuen, C.C. Teng, Y.L. Huang, I. Wang and M.H. Wei. Morphology, electrical, and pheological properties of silane-modified silver nanowire polymer composites, Macromol. Mater. Eng., 295, 2010, 2017-1024.

(14) S.S. Ray, and M. Okamato. Biodegradable polylactide and its nanocomposites: Opening a new dimension for plastics and composites, Macromol. Rapid Commun, 24, 2003, 815-840.

(15) B.S. Schwartz, C.L. Parker, J. Hess and H. Frumkin, Public health and medicine in an age of energy scarcity: The case of petroleum, Am. J. Public Health.,101, 2011, 1560-1567.

(16) J.M. Raquez, Y. Habibi, M. Murariu and P. Dubois. Polylactide (PLA)-based nanocomposites, Prog. Polym. Sci., 38, 2013, 1504-1542.

(17) J.A. Roether, A.R. Boccaccini, L.L. Hench, V.Maquet, S. Gautier and R. Jerome. Development and in vitro characterization of novel bioresorbable and bioactive composites materials based on polylactide foams and bioglass for tissue enginerring applications, Biomaterials, 23, 2002, 3871-3878.

(18) J.W. Rhim, S.I. Hong and C.S. Ha. Tensile, water vapor barrier and antibacterial properties PLA/nanoclay composite films, LWT-Food Sci. Technol., 42, 2009, 612-617.

(19) K.G. Nathalie, N. Gomez and C.E. Schmidt. Condcuting polymers in biomedical engineering, Prog. Poly. Sci., 32, 2007, 876-921.

(20) K. Kobashi, T. Villmow, T. Andres and P.Pötschke. Liquid sensing of melt-processed poly(lactic acid)/multi-walled carbon nanotube composite films, Sensor. Actuat. B-Chem., 134, 2008, 787-795.

(21) Y. Shen, T. Jing, W. Ren, J. Zhang, Z.G. Jiang, Z.Z Yu and A. Dasari. Chemical and thermal reduction of graphene oxide and its electrically conductive polylactic acid nanocomposites, Comp. Sci. Technol., 72, 2012, 1430-1435.

(22) E. Canessa, C. Fonda and M. Zennaro. Low-cost 3D printing for science, education & sustainable development. First ed, ICTP— The Abdus Salam International Center for Theoretical Physics, Italy, 2013.

(23) D.H. Rosenzweig, E. Carelli, T. Steffen, P. Jarzem and L. Haqlund. 3D-printed ABS and PLA scaffolds for cartilage and nucleus pulposus tissue regeneration, Int. J. Mol. Sci., 16, 2015, 15118-15135.

(24) S.J. Leigh, R.J. Bradley, C.P. Purssell, D.R. Bilson and D.A. Hutchins. A simple, low-cost conductive composite material for 3D printing electronic sensors *PLoS. One*, 7, 2012**,** e49365-.

(25) X. Wei, D.Li, W. Jiang, Z. Gu. X. Wang, Z. Zhang and Z. Sun, 3D printable graphene composite, Sci. Rep., 5, 2015, 5:11181.

(26) http://www.blackmagic3d.com/, 2016 (accessed 11.02.16).

(27) M.H.Hartmann. Biopolymers from renewable resources, In D.L. Kaplan Editor (Ed.) Springer-Verlag, Berlin, 1998, 367-411.

(28) K.M. Nampoothiri, N.R. Nair and R.P.John. An overview of recent developments in polylactide (PLA) reseach. Bioresource Technol., 11, 2010, 8493-8201.

(29) L. Xiao, B. Wang, G. Yang and M. Gauthier. Poly(Lactic Acid)-Based Biomaterials: Synthesis, In D. N. Ghista Editor (Ed.) Modification and Applications. Biomedical Science, Enginering and Technoogy, Intech, 2012 247- 282.

(30) D. Garlotta. A literature review of pol(lactic acid). J.Polym. Environ., 9, 2001, 63-84.

(31) US Patent No: 5142023 (1992), invs.: P. R. Gruber, E. S. Hall, J. H. Kolstad, M. L. Iwen, R. D. Benson, R. L. Borchardt.

(32) R. Auras, B. Harte and S. Selke. An Overview of Polylactides as Packaging Materials. Macromol. Biosci., 4, 2004, 835-864.

(33) H. Tsuji and Y. Ikada. Crystallization from the melt of poly(lactide)s with different optical purities and their blends. Macromol. Chem. Phys., 197, 1996, 3483-3499.

(34) D. R. Witzke,. Introduction to properties, engineering and prospectes of polylactide polymers, Ph.D Thesis. Michigan State University, East Lansing, 1997.

(35) S. Jacobsen, P. Degee, H.G. Fritz, P. Dubois and R. Jerome. Polylactide (PLA)-A new way of production. Polym. Eng. Sci, 39, 1999, 1311-1319.

(36) H.Balakrishnan, R. Hassan, M. Imran and M.U. Wahit, Toughening of Polylactic Acid Nanocomposites: A Short Review, Polym-Plast. Technol., 51, 2012, 175-192.

(37) G.Z. Papageorgiou, D.S. Achilias, S. Nanoki, T. Beslikas, and D. Bikiaris, PLA Nanocomposites: Effect of Filler Type on Non-Isothermal Crystalization. Thermochım. Acta, 511, 2010, 139.

(38) C.F. Kuan, H. C. Kuan, C.C. M. Ma and C.H. Chen, Mechanical and electrical properties of multiwall carbon nanotube/poly (lactic acid) composites, J. Phys. Chem. Solids, 69, 2008, 1395-1398.

(39) T. Willmow, P. Potschke, S. Pegel, L. Haussler and B. Kretzshmar, Influence of twin screw extrusion conditions on the dipersion of multi walled carbon nanotubes in a poly (lactic acid) matrix. Polymer, 49, 2008, 3500-3509.

(40) M. Raja and S.H. Shanmugharaj. Thermal, mechanical and electroactive shape memory properties of polyurethane/pol (lactic acid)/ CNT nanocomposites. Eur. Polym. J., 49, 2013, 3492-3500.

(41) X.P. Wei, Y.L. Luo, F. Xu and Y.S. Chen, Sensitive conductive polymer composites based on polylactic acid filled with multiwalled carbon nanotubes for chemical vapor sensing, Synthetic Met., 215, 2016, 216-222.

(42) A. K. Geim and K.S. Navoselov, The rise of graphene. Nat. Mater., 6 2007, 183-191.

(43) G. Wang, X. Shen, J. Yao and J. Park, Graphene Nanosheets for Enhanced Litium Storage in Lithium Ion Batteries. Carbon, 47, 2009, 2049-2053.

(44) Li D, Muller B, Gilje S, Kaner RB and Wallace GG. Processable aqueous dispersions of graphene nanosheets. Nat. Nanotechnol., 3, 2007, 101–5.

(45) Xu Y, Liu Z, Zhang X, Wang Y, Tian J, Huang Y, Ma Y, Zhang X, Chen Y. A graphene hybrid material covalently functionalized with porphyrin: synthesis and optical limiting property Adv. Mater., 21, 2009, 1275–9.

(46) I. H. Kim and Y.G. Jeong. Polylactide/exfoliated graphite nanocomposites with enhanced thermal stability, mechanical modulus, and electrical conductivity. J. Polym. Sci. Pol. Phys., 48, 2010, 850–8.

(47) M. Murariu, A.L. Dechief, L. Bonnaud, Y. Paint, A. Gallos, G. Fontaine, S. Bourbigot and Dubois. The production and properties of polylactide composites filled with expanded graphite. Polym. Degrad. Stabil, 95, 2010, 889–900.

(48) X. Xu, Q. Yang, Y. Wang, H. Yu, X. Chen and X. Jing. Biodegradable electrospun polylactide fibers containing antibacterial silver nanoparticles. Eur. Polym. J., 42, 2006, 2081-2087.

(49) E. Fortunati, I. Armentano, Q. Zhou, A. Iannoni, E. Saino, L. Visai, L.A. Berglund and J.M. Kenny. Multifunctional bionanocomposites films of PLA, cellulose nanocrystals and silver nanoparticles, Carbohyd. Polyme., 87, 2012, 1596-1605.

(50) F.Fievet, J.P. Lagier and M. Figlarz. Prepearing Monodispersed Metal Powders in Micronmeter and Submicronmeter Sizes by the Polyol Process, MRS Bull., 14, 1989, 29-34.

(51) J. Zhang, X. Li, X. Sun, and Y. Li. Surface Enhanced Raman Scattering Effects of Silver Colloids with Different Shapes, J. Phys. Chem. B., 109, 2005, 12544-12548.

(52) Y. Sun, B. Gates, B. Mayers and Y. Xia. Crystalline Nanowires by Soft Solution Processing, Nano Lett. 2, 2002, 165-168.

(53) B. Wiley, Y. Sun, B.Mayers and Y. Xia. Shape-Controlled Sythesis of Metal Nanostructures: The Case of Silver, Chem.-Eur. J., 11, 2005, 454-463.

(54) Y. Sun, B. Mayers, T. Herricks and Y. Xia. Polyol Sythesis of Unifrm Silver Nanowires: A Plausible Growth Mechnaism and the Supporting Evidence, Nano Letters, 3, 2003, 955-960.

(55) B. Wiley, Y. Sun and Y. Xia. Sythesis of Silver Nanostructures with Controlled Shapes and Properties. Acc. Chem. Res., 40, 2007, 1067-1076.

(56) S.I. White, P.M. Vora, J.M. Kikkawa, J.E. Fischer and K.I. Winey. Temperature- Dependent Resistive Switching in Bulk Silver Nanowire-Polystyrene Composites, J. Phys. Chem. C., 114, 2010, 22106-22112.

(57) A. Lonjon, P. Demont, E. Dantras, and C. Lacabanne. Low filled conductive P(VDF-TRE) composites: Influence of silver pacticles aspect ratio on percolation threshold from spheres to nanowires, J. Non-cryst. Solids, 358, 2012, 3074-3078.

(58) A. Lonjon, I. Caffrey, D. Carponcin, E. Dantas, C. Lacabanne. High electrically conductive composites of Polyamide 11 filled with silver nanowires: Nanocomposites processing, mechanical and electrical analysis. J. Non-cryst. Solids, 376, 2013, 199-204.

(59) I. Moreno, N. Navascues, M. Arruebo, S. Irusta and J. Santamaria. Facile preparation of transparent and conductive polymer films based on silver nanowire/polycarbonate nanocomposites, Nanotechnology, 24, 2013, 275603.

(60) M. Sureshkumar, H.Y. NA, K.H. Ahn and S.J. Lee. Conductive nanocomposites based on polystyrene microspheres and silver nanowires by latex blending, ACS Appl. Mater. Interfaces, 7, 2015, 756-764.

(61) Y. Wei, S. Chen, F. Li, K. Li and L. Kui. Hybrids of silver nanowires and silica nanoparticles as morphology controlled conductive filler applied in flexible conductive nanocomposites, Compos. Part. A-Appl. S., 73, 2015, 195-203.

(62) C. Kaynak, Y. Meyva. Use of maleic anhydride compatibilization to toughness and other properties of polylactide blended with thermoplastic elastomers. Polym. Adv. Technol., 25, 2014, 1622-1632.

(63) S. Coskun, B. Aksoy, and H.E. Unalan. Polyol synthesis of silver nanowires: An extensive parametric study, Cryst. Growth Des., 11, 2011, 4963-4969.

(64) J.W. Rhim, A.K. Mohanty, S.P.Singh and P.K.W. Ng. Effect of the processing methods on the performance of polylactide films: Thermocompression versus solvent casting, *J. Appl. Polym.* Sci., 101, 2006, 3736-3742.

(65) E.W. Fisher, H.J. Sterzel and G. Wegner. Investigation of the structure of solution grown crystals of lactide copolymers by means of chemical reactions. *Colloid Polym. Sci.*, 251, 1973, 980-990.

(66) T.B. Song, Y. Chen, C.H. Chung, Y. Yang, B. Bob, H.S. Duan, G. Li, K.N. Tu, Y. Huang and Y. Yang. Nanoscale joule heating and electromigration enhanced ripening of silver nanowire contacts, ACS Nano, 8, 2014, 2804-2811.

(67) M. Mahmoodi, Y.H. Lee, A. Mohamad, S.S. Park. Effect of flow ınduced alignment on the thermal conductivity of injection molded carbon nanotube filled polystyrene nanocomposites, Polym. Eng. Sci., 55, 2015, 753-762.

(68) L.J. Lanticse, Y.Tanabe, K. Matusi, Y. Kaburagi, K. Suda, M. Hoteida, M. Endo and, E. Yasseuda. Shear-induced preferential alignment of carbon nanotubes resulted in anisotropic electrical conductivity of polymer composites, Carbon, 44, 2006, 3078-3086.

(69) S. Coskun, E.S. Ates, H.E. Unalan. Optimization of silver nanowire networks for polymer light emitting diode electrodes, Nanotechnology, 24, 2013, 125202.

(70) E. Marzbanrad, G. Rivers, P. Peng, B. Zhao and Y. Zhou. How morphology and surface texture affect thermal stability of a metallic nanoparticle: the case of silver nanobelts and pentagonal silver nanowires, Phys. Chem. Chem. Phys., 17, 2015, 315-324.

(71) G. Boiteux, C. Boullanger, P. Cassagnau, R. Fulchiron and G. Seytre. Influence of morphologyon PTC in conducting polypropylene-silver composites. Macromol. Symp, 233, 2006, 246-253.

(72) S.L. Yang, Z.H.Wu, W. Yang and M.B. Yang, Thermal and mechanical properties of crosslinked polylactide (PLA), Polym. Test., 27, 2008, 957-963.

(73) Y. Borodko, S.E. Habas, M. Koebel, P. Yang, H. Frei, and G.A. Somorjai, Probing the interaction of poly /vinylpyrrolidone) with platinum nanocrystals by UV- Raman and FTIR, J.Phys. Chem. B., 110, 2006, 235052-23059.

(74) I. Balberg. Universal percolation-threshold limits in the continuum, Phys. Rev. B., 31, 1984, 4053-4055.

(75) I. Balberg, N, Binenbaum, and N. Wagner. Percolation threshold in the three-dimentional sticks system, Phys. Rev. Lett., 52, 1984, 1465-1468.

(76) K. Shinyama and S. Fujita, *IEEE 7th International Conference on Properties and Applications of Dielectric Materials*., 2003, 707-710.

(77) R.M. Motiso and K.I. Winey. Electrical properties of polymer nanocomposites containing rod-like nanofillers, Prog. Polym. Sci., 40, 2015, 63-84.

(78) S. Kirkpatrick. Percolation and conduction, Rev. Mod. Phys., 45, 1973, 574-588.

(79) J. Li and M.Östling, Conductivity scaling in supercritical percolation of nanoparticles- not apower law, Nanoscale, 7, 2015, 3424-3428.

(80) A.T. Bellew, H.G. Mannings, C. G. Rocha, M.S. Ferreira and, J. J. Boland, Resistance of single Ag nanowire junctions and hteir role in the conductivity of nanowire networks, ACS Nano, 9, 2015, 11422-11429.

(81) G. Gorrasi, R. Pantani, M. Murariu and P. Dunois, PLA/Halloysite Nanocomposite Films: Water Vapor Barrier Properties and Specific Key Characteristics, Macromol. Mater. Eng., 299, 2014, 104-115.

(82) E. Fortunati, I. Armentano, Q. Zhou, A. Iannoni, E. Saino, L. Visai, L.A. Berglund and J.M. Kenny, Multifunctional bionanocomposite films of poly(lactic acid), cellulose nanocrystals and silver nanoparticles, Carbohyd. Polym., 87, 2012, 1596-1605.

(83) G. Ozkoc and S. Kemaloglu, Morphology, biodegradability, mechanical and thermal properties of nanocomposite films based on PLA and plasticized PLA, J. Appl. Polym. Sci., 144, 2009, 2481-2487.

(84) Q. Shi, C. Zhou, Y. Yue, W. Guo, Y. Wu and Q. Wu, Mechanical properties and in vitro degradation of electrospun bio-nanocomposite mats from PLA and cellulose nanocrystal, Carbohyd. Polym., 90, 2012, 301-308.

(85) J.T. Yoon, Y. G. Jeong, S.C. Lee and B.G. Min, Influences of poly(lactic acid)-grafted carbon nanotube on thermal, mechanical and electrical properties of poly(lactic acid), Polym. Adv. Technol., 20, 2009, 631-638.

(86) A. M. Pinto, J. Cabral, D.A. P. Tanaka, A. M. Mendes, and F. D. Magalhes, Effect of incorporation of graphene oxide and graphene nanoplatelets on mechanical and gas permeability properties of poly(lactic acid) films, Polym. Int., 62, 2013, 33-40.

(87) C. Kaynak, and I. Kaygusuz, Consequences of accelerated weathering in polylactide nanocomposites reinforced with halloysite nanotubes, J. Compos. Mater., 50, 2015, 365-375.

(88) M. Jonoobi, J. Harun, A.P. Mathew and K. Oksman, Mechanical properties of cellulose nanofiber (CNF) reinforced polylactic acid (PLA) prepared by twin screw extrusion, Compos. Sci. Technol., 70, 2010, 1742-1747.